

# GRID-independent molecular descriptor analysis and molecular docking studies to mimic the binding hypothesis of $\gamma$ -aminobutyric acid transporter 1 (GAT1) inhibitors

Sadia Zafar\* and Ishrat Jabeen\*

Research Center for Modeling and Simulation (RCMS), National University of Sciences and Technology (NUST), Islamabad, Federal, Pakistan

\* These authors contributed equally to this work.

## ABSTRACT

**Background:** The  $\gamma$ -aminobutyric acid (GABA) transporter GAT1 is involved in GABA transport across the biological membrane in and out of the synaptic cleft. The efficiency of this  $\text{Na}^+$  coupled GABA transport is regulated by an electrochemical gradient, which is directed inward under normal conditions. However, in certain pathophysiological situations, including strong depolarization or an imbalance in ion homeostasis, the GABA influx into the cytoplasm is increased by re-uptake transport mechanism. This mechanism may lead to extra removal of extracellular GABA which results in numerous neurological disorders such as epilepsy. Thus, small molecule inhibitors of GABA re-uptake may enhance GABA activity at the synaptic clefts.

**Methods:** In the present study, various GRID-independent molecular descriptor (GRIND) models have been developed to shed light on the 3D structural features of human GAT1 (hGAT1) inhibitors using nipecotic acid and N-diarylalkenyl piperidine analogs. Further, a binding hypothesis has been developed for the selected GAT1 antagonists by molecular docking inside the binding cavity of hGAT1 homology model.

**Results:** Our results indicate that two hydrogen bond acceptors, one hydrogen bond donor and one hydrophobic region at certain distances from each other play an important role in achieving high inhibitory potency against hGAT1. Our docking results elucidate the importance of the COOH group in hGAT1 antagonists by considering substitution of the COOH group with an isoxazol ring in compound **37**, which subsequently leads to a three order of magnitude decrease in biological activity of **37** ( $\text{IC}_{50} = 38 \mu\text{M}$ ) as compared to compound **1** ( $\text{IC}_{50} = 0.040 \mu\text{M}$ ).

**Discussion:** Our docking results are strengthened by the structure activity relationship of the data series as well as by GRIND models, thus providing a significant structural basis for understanding the binding of antagonists, which may be useful for guiding the design of hGAT1 inhibitors.

Submitted 11 October 2018  
Accepted 14 December 2018  
Published 31 January 2019

Corresponding author  
Ishrat Jabeen,  
ishrat.jabeen@rcms.nust.edu.pk

Academic editor  
Joao Rocha

Additional Information and  
Declarations can be found on  
page 25

DOI 10.7717/peerj.6283

© 2019 Zafar and Jabeen

Distributed under  
Creative Commons CC-BY 4.0

OPEN ACCESS

**Subjects** Computational Biology, Neuroscience, Pharmacology

**Keywords** 3D QSAR, GRIND model, GABA transporter 1 (GAT1), Tiagabine, hGAT1 inhibitors, Docking, Structure–activity relationship (SAR)

## INTRODUCTION

Brain functioning is controlled by neuron circuits that release excitatory and inhibitory neurotransmitters like glutamate and  $\gamma$ -aminobutyric acid (GABA) and neuromodulators like norepinephrine, dopamine and serotonin (Heng, Moonen & Nguyen, 2007).

The removal of neurotransmitters from the extracellular space (i.e., between pre- and post-synaptic neurons) is regulated by their respective transporters (Calapai et al., 2001). However, imbalances in the levels of these neurotransmitters at synaptic clefts which may be associated with several neurological disorders, including Alzheimer's disease, schizophrenia, Parkinson's disease, anxiety, sleep disorders and epilepsy (Sherin & Nemeroff, 2011; Pirttimaki, Parri & Crunelli, 2013; Shetty & Bates, 2015). Most of these neurological disorders are associated with the GABAergic system and are mainly modulated using allosteric agonists of the GABAA receptor. However, inhibition of the GABA re-uptake transport to maintain its concentration gradient at synaptic clefts represents a promising concept for treating neurological disorders (Carvill et al., 2015).

GABA transporters (GATs) are categorized into four subtypes, GAT1-3, and betaine/GABA transporter 1 (BGT1) (Jin et al., 2011). GAT1 and 3 are mainly expressed at GABAergic neurons and glial cells, respectively, throughout the brain (Minelli et al., 1995; Minelli et al., 1996; Conti et al., 1998; Melone, Ciappelloni & Conti, 2015). However, GAT2 is localized at arachnoid and ependymal cells and has very low expression in neurons and glial cells in the brain (Conti et al., 1999; Jin et al., 2011); BGT1 is expressed, from low to high concentration, in the liver, kidney, meninges and at the blood brain barrier (Anderson, Kidd & Eskandari, 2010). All GATs belong to the neurotransmitter sodium symporter family. These transporters use a sodium gradient for re-uptake of the neurotransmitters out of the synaptic cleft; however, in certain cases a reverse transport mode is also known, which releases the neurotransmitter in a nonvesicular way (Yu et al., 1998). Overall, 75% of GABA re-uptake is mediated by GAT1 (Parpura & Haydon, 2008; Zafar & Jabeen, 2018). This reflects that GAT1 is mainly accountable for GABA transport and related disorders. Therefore, development of potential antagonists of this transporter to maintain the concentration gradient of GABA at synaptic clefts may represent a potential therapeutic strategy. Up to now, Tiagabine is the only second-generation FDA approved anticonvulsant agent that selectively inhibits *Homo sapiens* GAT1 (hGAT1). However, Tiagabine analogs that have been developed are often associated with off target toxicity and poor ADME-Tox properties that lead to side effects such as sedation, tremors and ataxia (Madsen et al., 2011). Thus, developing new chemical scaffolds of GABA reuptake inhibitors (i.e., hGAT1 antagonists) that have maximum efficacy and reduced toxicity might aid in the successful treatment of neuronal disorders.

Previously, various antagonists of hGAT1, including nipecotic acid, guvacine, proline, pyrrolidine, azetidine and THPO derivatives (Dalby, 2000; Andersen et al., 2001; Clausen et al., 2005; Fülep et al., 2006; Faust et al., 2010; Hellenbrand et al., 2016; Schmidt, Höfner & Wanner, 2017; Lutz et al., 2018; Tóth, Höfner & Wanner, 2018), have been synthesized and pharmacologically tested and optimized using structure-activity

relationship (SAR) data. Additionally, several ligand-based strategies including 2D QSAR (Jurik *et al.*, 2013), CoMFA (Zheng *et al.*, 2006) and pharmacophore models (Hirayama, Díez-Sampedro & Wright, 2001; Nowaczyk *et al.*, 2018) have been developed to optimize small molecule inhibitors against hGAT1. However, most of these studies were class specific, focusing on nipecotic acid derivatives (Petrera *et al.*, 2015), Tiagabine analogs (Jurik *et al.*, 2015) and triaryl nipecotic acid derivatives (Dhar *et al.*, 1994). Recently, a nipecotic acid derivative DDPM-2571 has been synthesized with one log unit greater inhibitory potency against GAT1 as compared to Tiagabine which showed anticonvulsant, antidepressant and antinociceptive effects in mouse models (Salat *et al.*, 2017). Moreover, a novel class of allosteric GAT1 antagonists has been identified through mass spectrometry screening of pseudostatic hydrazone libraries. Hauke *et al.* (2018) suggested that the identified allosteric nipecotic acid derivatives may provide physiological relevance in terms of hGAT1 modulation as their interaction in hGAT1 binding pocket differs from Tiagabine. Additionally, some reports also suggest 5-aminolevulinic acid (5-Ala) may also inhibit the cellular uptake of GABA by GAT isoforms (Rud *et al.*, 2000). Until very recent, no X-ray crystal structure of any hGAT has been published. Therefore, various hGAT1 models in different conformations have been developed previously using the crystal structure of the leucine transporter (LeuT) from *Aquifex aeolicus* (PDB ID: 3F3A) as a template. These models may assist to study the binding of hGAT1 antagonists and to study the ion dependent transport mechanistic of GABA through hGAT1 (Bicho & Grewer, 2005; Jurik *et al.*, 2015).

In the present study, we aim to develop predictive GRID-independent molecular descriptor (GRIND) models to provide deeper insight into the 3D structural features of hGAT1 antagonists. Moreover, a recently published X-ray structure of dopamine transporter (DAT) in *Drosophila melanogaster* (dDAT, PDB ID: 4XP4, resolution: 2.8 Å, sequence identity: 46%) (Wang, Penmatsa & Gouaux, 2015b) is used in the current study to build a model of hGAT1, followed by molecular docking studies to probe how nipecotic acid and N-diarylalkenyl piperidine analogs bind to the binding cavity of hGAT1.

## METHODS

### Dataset

A complete workflow of hGAT1 antagonists data pre-processing and cleaning has been provided in Fig. 1. Briefly, a dataset of 580 hGAT1 antagonists, along with their respective binding affinities (IC<sub>50</sub>) ranging from 0.04 to 8511 μM, was obtained from the literature (Dhar *et al.*, 1994; Schousboe, 2000; Clausen *et al.*, 2005, 2006; Fülep *et al.*, 2006; Zheng *et al.*, 2006; Alexander, Mathie & Peters, 2007; Reith, 2007; Faust *et al.*, 2010; Alexander, Mathie & Peters, 2011; Nakada *et al.*, 2013; Quandt, Höfner & Wanner, 2013; Sitka *et al.*, 2013). Subsequently, duplicates and fragments were removed from the data, followed by the removal of antagonists with a molecular mass less than 150 and IC<sub>50</sub> >100 μM. The duplicate antagonists were the replicated chemical compounds with biological activities determined through different biological assays including [<sup>3</sup>H] GABA uptake assay, GAT1 transport assay, radio-ligand binding assay and equilibrium

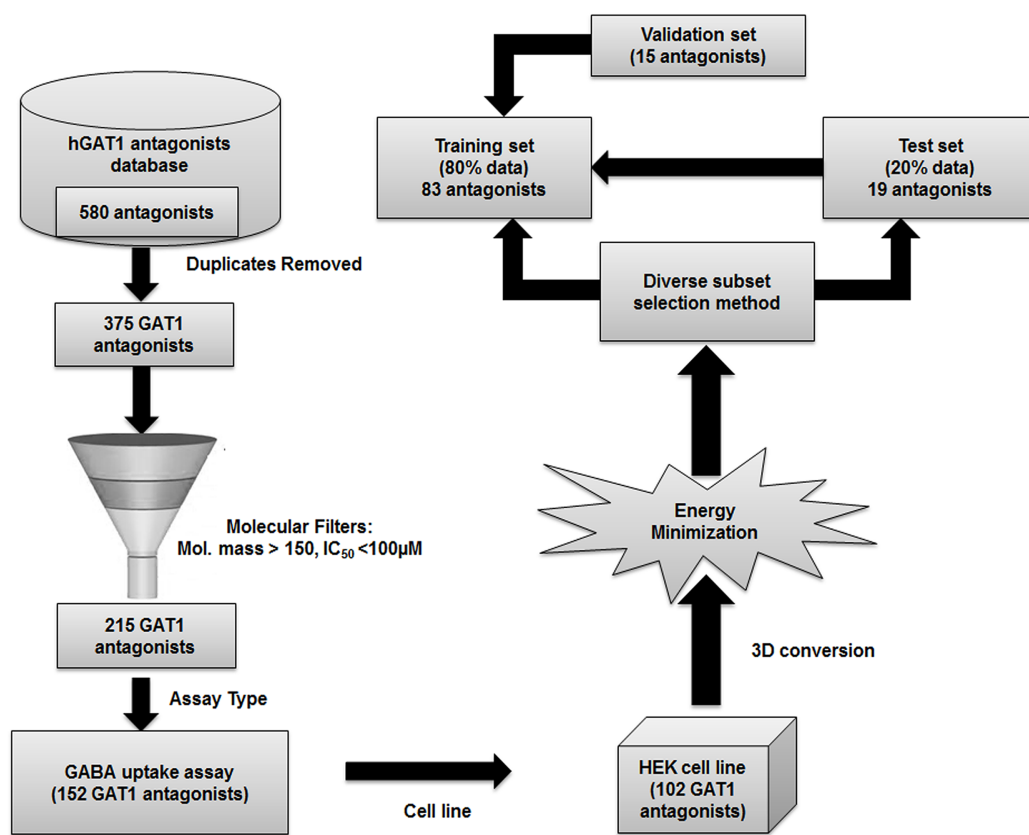


**Figure 1** Workflow of the hGAT1 antagonists data pre-processing and cleaning.

Full-size DOI: 10.7717/peerj.6283/fig-1

binding assay using different expression systems like *Xenopus* oocytes and HEK cell lines (Dhar *et al.*, 1994; Kragler, Höfner & Wanner, 2008; Nakada *et al.*, 2013). Moreover, the antagonists with molecular mass less than 150 were excluded from the analysis because they were representing molecular fragments and therefore may not be selective against the hGAT1. Similarly, antagonists with  $IC_{50} > 100 \mu\text{M}$  were also discarded as they reflect least active compounds in comparison with the most active antagonist of the database ( $IC_{50} = 0.040 \mu\text{M}$ ). Thus, only the data with  $IC_{50}$  values ranging from 0.040 to 100  $\mu\text{M}$  was used for further analysis. Overall, our data comprises of total 215 antagonists that were further subjected to biological cleaning by selecting only those antagonists whose  $IC_{50}$  values were evaluated using a radio labeled [3H] GABA uptake assay (152 antagonists) in hGAT1 expressing HEK cells (102 antagonists). Furthermore, 3D structures of the selected 102 antagonists (Table S1) were constructed and energy minimized using the MMFF94x force field (Halgren, 1996) in MOE version 2013.0802 (Chemical Computing Group, 2013). The final data set of the 102 antagonists of hGAT1 consists of nipecotic acid, proline, pyrrolidine, exo-THPO and N-diarylalkenyl piperidine derivatives that follow a general pattern of attachment of a COOH group at the ortho, meta or para positions of piperidine, proline, pyrrolidine, or azetidine rings, followed by a linker region of variable lengths. The general architecture of hGAT1 antagonists in the present data set is

represented in Fig. S1. It has been reported previously that attachment of aromatic moieties to the linker region is highly correlated with the activity of hGAT1 antagonists (Faust *et al.*, 2010). Depending on the type of cyclic moieties attached at the linker region, the present data set of hGAT1 antagonists was divided into three main classes (classes A, B and C). Overall, the whole data set of 102 hGAT1 inhibitors in Table S1 was further divided into a training set (80%) and a test set (20%) by using the diverse subset selection method (Schmucker, Givehchi & Schneider, 2004; Gillet, 2011). Briefly, 300 2D as well as 3D descriptors available in MOE version 2013.0802 (Chemical Computing Group, 2013) were computed to obtain a distance calculation for each database entry. 20% of the data structures (19 compounds) with larger distance values from each other were selected as the test set and the remaining 83 compounds (80%) were used to train the model (Minh, Klaere & von Haeseler, 2009) using GRIND (Durán & Pastor, 2011). Additionally, a recently published data set of 15 nipecotic acid derivatives was used as validation set (Lutz *et al.*, 2017).

### GRID-independent molecular descriptor

It has been previously reported that GRIND variables are highly dependent on the 3D conformations of molecules (Durán & Pastor, 2011). Therefore, multiple conformational search approaches were used to generate four different 3D conformational sets of the training data. Subsequently, each independent sets of molecular conformations, including energy minimized, extended 3D, induced fit docking (IFD) solutions, and molecular alignment conformations by pharmacophore mapping approach of hGAT1 antagonists along with their  $-\log IC_{50}$  values, were independently loaded into the software package Pentacle v 1.06 (Durán & Pastor, 2011) for the construction of four different GRIND models. Various authors have demonstrated that hGAT1 antagonists bind in their protonated state (Jurik *et al.*, 2015). Therefore, all the compounds in the different conformational sets were protonated at a physiological pH of 7.4. A complete protocol to train the 3D QSAR model using GRIND is provided in Fig. S2. Briefly, includes following steps:

1. **Computation of the molecular interaction fields (MIFs):** MIF computation was done using four different probes including DRY (hydrophobic probe), TIP (steric hot-spot defining molecular shape), N1 (hydrogen bond acceptor) and O (hydrogen bond donor) within a molecule. The total energy at each node was calculated as a sum of the Lennard-Jones potential ( $E_{lj}$ ) (Lennard-Jones, 1931; Bouanich, 1992), the electrostatic energy ( $E_{el}$ ), and the hydrogen bond energies ( $E_{hb}$ ) by iteratively placing each probe at different GRID steps:

$$E_{xyz} = \sum E_{lj} + \sum E_{el} + \sum E_{hb}$$

2. **Discretization:** AMANDA algorithm (Durán, Martínez & Pastor, 2008) was used to discretize the MIFs using default energy cutoff values of  $-0.75$ ,  $-0.5$ ,  $-4.2$  and  $-2.6$  for the TIP, DRY, N1 and O probes, respectively, to pre-filter the nodes that fails to meet the energy cutoffs.

3. **Encoding:** The consistently large auto and cross correlation algorithm (*Durán & Pastor, 2011*) with default parameters was used for the encoding of the pre-filtered nodes at each discretization step. This produces consistent sets of variables whose values are directly represented in the form of correlogram plots. To correlate the structural variance of the training set data with respective biological activity ( $-\log IC_{50}$ ), a partial least square (PLS) analysis has been performed using the full set of 570 active GRIND variables for each model. Moreover, to remove the inconsistent set of variables, cycles of fractional factorial design (FFD) (*Baroni et al., 1993*) were employed to obtain a good statistical model.

## Multiple conformational analysis

### *Standard 3D conformations*

Software CORINA v4.1.0 (*Sadowski, 2003*) was used to generate standard 3D conformations of the molecules. Briefly, CORINA build the 3D model of a molecule by combining the monocentric fragments with standard bond lengths, bond angles and dihedral angles, including the torsion angles of ring systems for their proper closure and to minimize the non-bonded (Van der Waals and electrostatic) interactions that occur within the flexible parts of the molecules (*Sadowski, Schwab & Gasteiger, 2004*). Finally, generated standard 3D conformation of each hGAT1 antagonist in the data set was further subjected to Pentacle v 1.06 (*Durán & Pastor, 2011*) for GRIND analysis.

### *Energy minimized conformations*

The stochastic search algorithm in MOE v2013.0802 (*Chemical Computing Group, 2013*) was used to produce energy minimized conformations of the hGAT1 antagonists. A total of 250 conformations were generated and ranked according to their energy values. Each individual in the data set with the lowest energy score was selected for the GRIND analysis.

### *Induced fit docking (IFD)*

The IFD (*Sherman et al., 2006*) protocol in MOE v2013.0802 (*Chemical Computing Group, 2013*) was followed to generate the docking solutions of 102 hGAT1 antagonists within the binding pocket of the hGAT1 model. The binding cavity was selected to include the residues already known to be involved in ligand-protein interactions in hGAT1, i.e., G59, Y60, A61, I62, G63, G65, N66, W68, Y86, L136, Y139, Y140, I143, Q291, F294, S295, Y296, G297, L300, N327, S328, S331, A358, L392, D395, S396 and D451 (*Zhou, Zomot & Kanner, 2006*; *Skovstrup et al., 2010*; *Jurik et al., 2015*). Overall, 20 poses per ligand were generated using default scoring function (London dG) and placement method (Triangle Matcher). Finally, the best scored docking conformation for each ligand was selected for further GRIND analysis.

### *Pharmacophore mapping approach*

Another set of molecular conformations was generated by the pharmacophore mapping approach (*Martin et al., 1993*) using MOE v2013.0802 (*Chemical Computing Group, 2013*). Briefly, the standard 3D conformation of the prototype ligand Tiagabine was used as a

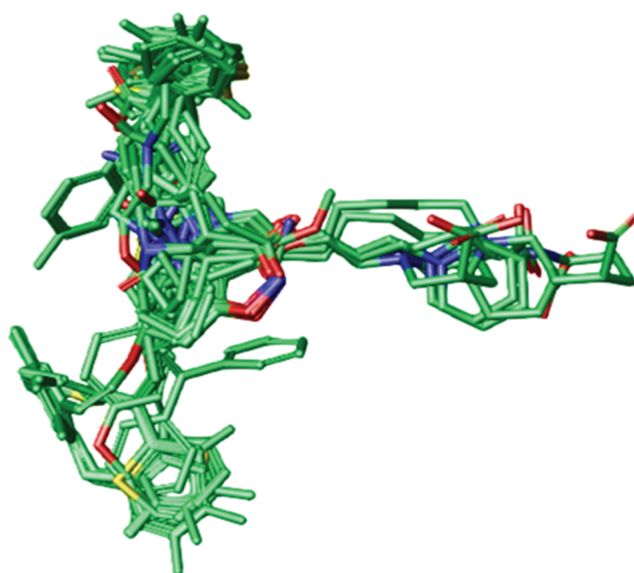


**Figure 2** Best aligned conformations of complete data set (102 compounds) of hGAT1 antagonists on standard 3D conformation of Tiagabine as a template. Full-size  DOI: 10.7717/peerj.6283/fig-2

template for the flexible alignment of the rest of the data. The best scored aligned system based on the energy values, shown in Fig. 2, was selected to develop the GRIND model.

Overall, the relevance of structural properties to the binding affinity has been determined by PLS analysis. However, the value of the correlation coefficient ( $R^2$ ) for the external test set validation was determined through Eq. 1 as described by Alexander, Tropsha & Winkler (2015).

$$R^2 = \frac{\sum (y - \hat{y})^2}{\sum (y - \bar{y})^2} \quad (1)$$

Where  $y$  represents the experimentally determined biological activity ( $-\log IC_{50}$ ) of the data set,  $\bar{y}$  is its mean value and  $\hat{y}$  represent the corresponding predicted biological activity ( $-\log IC_{50}$ ) by the GRIND model. The highly predictive final GRIND model helps to identify the 3D structural features of hGAT1 antagonists. However, in order to get deeper insight into the ligand interaction profiles within the hGAT1 binding site, further structure-based studies have been performed.

### Homology modeling

Due to the absence of a crystal structure of hGAT1, comparative modeling was performed using the recently solved crystal structure of the DAT in *D. melanogaster* (dDAT, resolution: 2.80 Å, PDB ID: 4XP4) (Wang, Penmatsa & Gouaux, 2015a). Comparative modeling of hGAT1 was performed using Modeller 9v8 software (Šali et al., 1995). Briefly, the primary sequence of hGAT1 (P30531) was retrieved from the UniProt KB databank (Magrane, 2011). Homologous transporter proteins include the LeuT and the DAT in the bacteria *A. aeolicus* (Yamashita et al., 2005) and *D. melanogaster*, respectively (Wang, Penmatsa & Gouaux, 2015a). Therefore, the homologous protein

dDAT (PDB ID: 4XP4) in an open-to-out conformation was selected as a template for multiple sequence alignment (Schrödinger, 2017) because it shares 46% sequence identity with hGAT1 as identified by BLASTp algorithm against the Protein Data Bank database (<https://blast.ncbi.nlm.nih.gov/>), compared to AaLeuT, which only shares 25% sequence identity with hGAT1. Additionally, dDAT also contains a Cl<sup>-</sup> ion, which is necessary to maintain the ionic concentration gradient in mammalian GABA transport (Wang, Penmatsa & Gouaux, 2015b). In contrast, in AaLeuT, the Cl<sup>-</sup> ion was not co-crystallized.

Flanking regions of the N- and C-terminus of hGAT1 were removed from the hGAT1 model built via Modeller 9v8 (Šali et al., 1995). However, no residues were trimmed from the extracellular loop 2 (EL2) of hGAT1, as was done in previously reported studies, due to the difference in the number of amino acid residues in EL2 for AaLeuT and hGAT1 (Baglo et al., 2013). The sodium ions and a chloride ion in a stoichiometry of 2:1 were added at the positions seen in dDAT. Briefly, 100 models of hGAT1 were built and the quality of these models was evaluated through ERRAT (Colovos & Yeates, 1993), PROCHECK (Lovell et al., 2003) and Verify3D (Bowie, Luthy & Eisenberg, 1991; Luthy, Bowie & Eisenberg, 1992) using the web server at <http://servicesn.mbi.ucla.edu/>. The final model was energy minimized using the MMFF94x force field of LigX (Labute, 2008) in MOE v2013.08 (Halgren, 1996). Finally, the model quality was again evaluated using a Ramachandran plot (Ho & Brasseur, 2005).

### Docking and pose analysis of selected hGAT1 modulators

Molecular docking was performed to get deeper insights into the binding of hGAT1 antagonists using GOLD suite v5.2.2 (Jones, Willett & Glen, 1995). To remove any bias in the pose generation step, different rotamers of the side chains were sampled. However, the ligand binding site was kept flexible. The binding site was sampled by keeping a distance of 17 Å around the amino acid residues G59, Y60, A61, I62, G63, G65, N66, W68, Y86, L136, Y139, Y140, I143, Q291, F294, S295, Y296, G297, L300, N327, S328, S331, A358, L392, D395, S396 and D451. These amino acid residues are already known from mutagenesis data to be important in interactions within hGAT1 (Zhou, Zomot & Kanner, 2006; Skovstrup et al., 2010; Jurik et al., 2015). Additionally, 2 Na<sup>+</sup> ions and a Cl<sup>-</sup> ion that are known for their role in the GABA transport mechanism were also incorporated into the binding cavity (Zhou, Zomot & Kanner, 2006; Skovstrup et al., 2010; Jurik et al., 2015). The side chains of hGAT1 (with the exception of ligand binding site residues) were kept rigid while the antagonists were treated flexible by performing 100 genetic algorithm runs per molecule using the gold score fitness function (Jones, Willett & Glen, 1995). The best pose for each ligand inside the hGAT1 binding pocket was selected for further ligand–protein interaction analysis.

To illustrate the binding hypothesis for hGAT1 antagonists with chemically different scaffolds, the docking solutions of selected compounds from each class, including compounds **2**, **6**, **8**, and **15** from class A, compounds **14**, **27**, **36**, and **40** from class B and compounds **1**, **3**, **4**, **37**, and **84** from class C were used for further hierarchical clustering analysis based on the root mean square deviation (RMSD) of the common scaffold



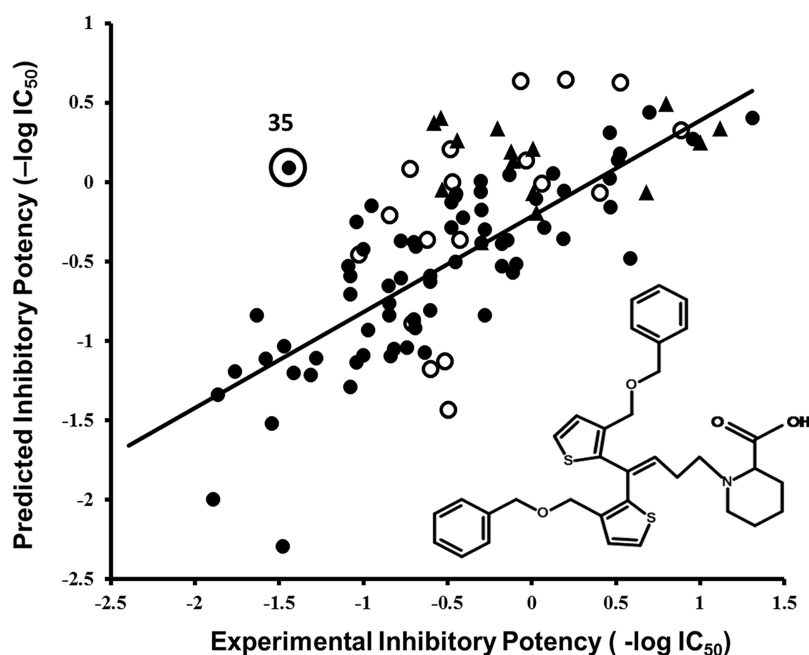


**Figure 3** Correlation plot between experimental versus predicted inhibitory potencies ( $-\log IC_{50}$ ) of hGAT1 antagonists. Training set, test set and validation set are represented with filled circles, hollow circles and triangles, respectively. The chemical structure represents observed outlier (compound 35) in the training set. [Full-size](#) DOI: 10.7717/peerj.6283/fig-3

(Stanton *et al.*, 1999) of each respective antagonist class. The compound selection criteria were solely based on the SAR data, as explained in the 'Results' section. A complete docking and pose selection protocol is provided in Fig. S3. Overall, a total of 172, 110 and 64 clusters were obtained for classes A, B and C, respectively, at 2 Å on the basis of the RMSD of the heavy atoms of the common scaffold (Stanton *et al.*, 1999). Final cluster of binding poses from each class was further selected on the basis of SAR data as explained in results section.

## RESULTS

### GRID-independent molecular descriptor (GRIND) analysis

The statistical parameters for each GRIND model developed from different conformational set are shown in Table S2. Unfortunately, none of the four conformational sets of ligands produced a statistically good model with the full set of variables. Thus, FFD (Baroni *et al.*, 1993) was applied to reduce the number of inconsistent variables in each model. After the first cycle of FFD, the statistical parameters of each model were slightly improved. However, a final model with good statistical parameters ( $q^2 = 0.59$ ,  $r^2 = 0.75$  and SDEP = 0.44) (Table S2) was obtained after two cycles of FFD with the pharmacophore-based aligned set of conformations on Tiagabine template.

Multiple linear regression analysis using leave one out cross validation (Elisseff & Pontil, 2003) of the final model resulted in a plot of observed versus predicted inhibitory potencies ( $-\log IC_{50}$ ) of the training data, as shown in Fig. 3. All the compounds in the training set (filled circles), test set (hollow circles) and validation set (triangles) are

well-predicted, with a difference of less than one log unit between the observed and the predicted biological activity values with the exception of compound **35**, for which the predicted activity ( $-\log IC_{50}$ ) value is 1.52 log units greater as compared to experimental activity value (Fig. 3). However, no outlier has been identified in the test set ( $R^2$ : 0.53, Table S3) and the validation set ( $R^2$ : 0.57). Briefly, the higher predicted activity value for compound **35** (actual  $-\log IC_{50}$ /predicted  $-\log IC_{50}$ : -1.44/0.08) (outlier in Fig. 3) is may be due to its high lipophilicity ( $\log P = 7.80$ ) which may lead to poor bioavailability and thus, overall poor experimental efficacy.

Figure 4A shows PLS coefficients correlograms of the final GRIND model. Positive and negative peaks in auto and cross correlograms of different variables (O, N1, DRY and TIP) elucidate their positive or negative contributions, respectively, towards the inhibitory potency ( $-\log IC_{50}$ ) against hGAT1. Additionally, it depicts the 3D structural features and their mutual distances that best describe their roles in the inhibition of hGAT1. It is evident from the PLS co-efficient correlogram that the O–O, N1–N1, DRY–N1, O–N1 and TIP–TIP variables have major influences on the inhibitory potency of the data set.

N1–N1 variables in Fig. 4A depict the presence of two hydrogen bond acceptor groups within the molecules that are present at a mutual distance of 8.00–8.40 Å in highly active (0.049–0.75 μM) antagonists of hGAT1. In the current data set, it represents a distance between the carbonyl and hydroxyl groups of the COOH attached at the ortho, meta and para positions of the piperidine ring in the nipecotic acid derivatives, as shown in Fig. 4B. All the compounds in the present data set (classes A, B and C) possess COOH groups attached at the ortho, meta or para positions of the piperidine ring. Compound **37** in class C is the only exception, where the COOH group has been substituted with an isoxazol ring. The N1–N1 correlogram for compound **37** represents a distance of 8.00–8.40 Å between the tertiary nitrogen of the piperidine ring and the carbonyl group of the isoxazol ring. Additionally, the N1–N1 pair of variables at a longer distance range of 14.00–14.40 Å shows a negative contribution towards the hGAT1 inhibition potential and, thus, has been identified in the least active (5.00–38 μM) compounds in the data set. Briefly, it represents a distance between the carbonyl oxygen of the COOH group and the ether group present either in the linker region or in the bulky aromatic substituents, as shown in Fig. 4C.

Interestingly, a sharp positive peak in the O–N1 correlogram in Fig. 4A demonstrates that a hydrogen bond acceptor at a distance of 5.60–6.00 Å from a hydrogen bond donor region has a positive effect on the inhibitory potency against hGAT1. Within the present data set, the hydrogen bond donor region represents the protonated nitrogen of the piperidine ring, while the COOH group provides the hydrogen bond acceptor region, as shown in Fig. 4D. This distance has been identified in the most active (0.049–0.75 μM) hGAT1 antagonists and is absent in the least active (5.00–38 μM) antagonists. This further strengthens the importance of the carbonyl group and the protonated nitrogen for the high inhibitory potency of hGAT1 antagonists. Additionally, the O–N1 pair of probes at a larger distance range of 10.40–10.80 Å, as shown in Fig. 4E, has been identified in the least active (6.56–78 μM) compounds within the data series and, thus, has a negative effect on the overall inhibitory potency against hGAT1. In the present

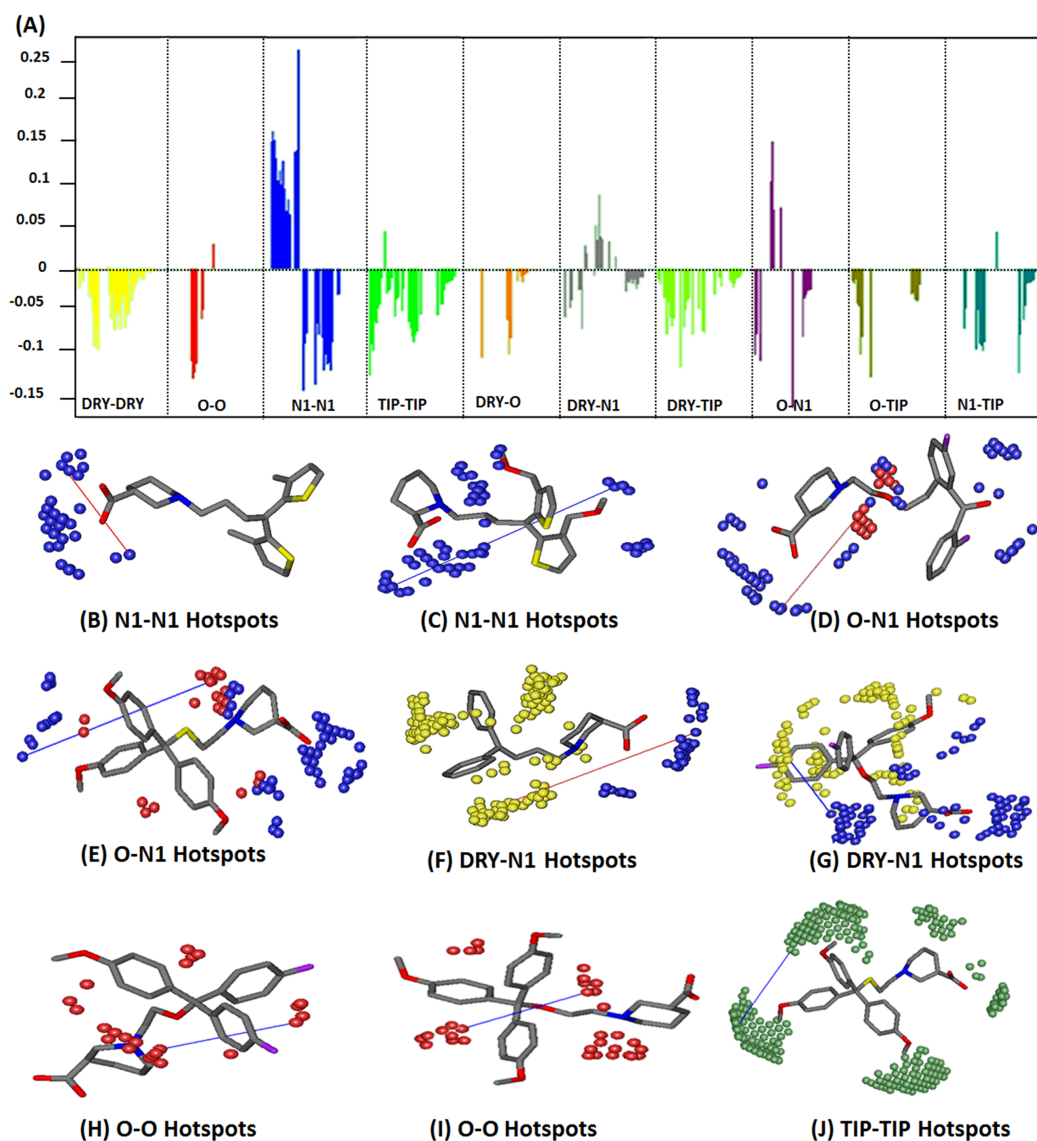


**Figure 4** (A) PLS coefficients correlograms showing the descriptors directly (positive value) or inversely (negative values) correlated to  $-\log IC_{50}$  values of the dataset. A change in biological activity against hGAT1 is depicted by N1-N1, O-N1, DRY-N1, TIP-TIP and O-O variables. (B) N1-N1 probes (blue contours) represents two hydrogen bond acceptor groups (OH and carbonyl group of COOH) at a mutual distance of 8.0–8.40 Å within highly active ligands (0.049–0.75 μM) whereas (C) represent N1-N1 pair of probes at a distance of 14.00–14.40 Å in least active compounds (5.00–38 μM) (D) reflects O-N1 pair of variable depicting a hydrogen bond donor (O: red contour) and a hydrogen bond acceptor (N1: blue contour) at a mutual distance of 5.60–6.00 Å within the highly active molecules (0.049–0.75 μM) while (E) represents O-N1 variable contours at a distance of 10.40–10.80 Å from each other in least active compounds (5.00–38 μM) (F) represent DRY-N1 pair of probes delineating a hydrophobic (DRY: yellow contour) at a distance of 10.40–10.80 Å from a hydrogen bond acceptor region (N1: blue contour) in the active ligands (0.049–0.75 μM) (G) represent DRY-N1 pair of probe at distance of 6.40–6.80 Å in least active compounds (4.34–78 μM) (H, I) represent O-O variables depicting two hydrogen bond donor probes (O: red contours) at a mutual distance of 6.00–6.40 Å within the molecules; (J) TIP-TIP pair of variable represent two molecular boundaries (green contours) at a mutual distance of 12.40–12.80 Å.

Full-size DOI: 10.7717/peerj.6283/fig-4

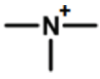
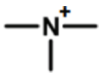
data series, this represents a distance between the protonated nitrogen (hydrogen bond donor) of the piperidine ring and the methoxy substitution of the diaryl moieties (hydrogen bond acceptor), as shown in Fig. 4E. Previously, the importance of the protonated nitrogen group in the piperidine ring of hGAT1 antagonists has been demonstrated by Zheng *et al.* (2006) by CoMFA analysis of N-diarylalkenyl-piperidinecarboxylic acid analogs. Thus, it is tempting to speculate that the methoxy groups at the N-diarylalkenyl rings in the data series may have a negative effect on the inhibitory potency against hGAT1.

Similarly, the DRY–N1 pair of probes in Fig. 4A represents one hydrophobic region (DRY) and one hydrogen bond acceptor variable region within the molecules (N1). Both features have been identified at a mutual distance of 10.40–10.80 Å in highly active compounds (0.049–0.75 µM) and at a distance of 6.40–6.80 Å in the least active compounds (4.34–78 µM). In highly active compounds, this represents the distance between aromatic moieties (thiophene rings, benzene rings and tricyclic rings) and the COOH group at the piperidine, proline, pyrrolidine, or azetidine ring, as shown in Fig. 4F. However, in the least active compounds it represents a distance between the aromatic moieties and the ether group in the linker region, as shown in Fig. 4G. Interestingly, all the selected compounds of classes A, B and C follow the distance pattern of highly active compounds in the DRY–N1 correlogram. Moreover, compound 37 (IC<sub>50</sub> = 38 µM) of class C shows a distance of 6.40–6.80 Å between the carbonyl group of the isoxazol ring and the benzene ring substituent at the linker region, which may provide a reason for the low biological activity of compound 37.

Furthermore, the O–O correlogram in Fig. 4A shows the presence of two hydrogen bond donors at a mutual distance of 6.00–6.40 Å within the least active (10–78 µM) compounds and, thus, may contribute negatively towards the inhibitory potency of the data set against hGAT1. For instance, in compound 32 this distance is associated with the ether group present in the hydrophilic chain and the para-monofluoro groups attached to the aromatic rings, as shown in Fig. 4H. Thus, it may be inferred that attachment of any electronegative atom to the ortho or para positions of the aromatic moieties is not favorable for achieving high biological activity values in this data series. Similarly, another example of the O–O correlogram is presented by compound 36 of class B, for which this variable represents the distance between the ether linker region of the hydrophilic chain and the para-methoxy group attached at the R<sub>2</sub> group, as shown in Fig. 4I.

Furthermore, the TIP–TIP correlogram in Fig. 4A represents two molecular boundaries of methoxy substitutions on the aromatic moieties at a mutual distance of 12.40–12.80 Å in the least active compounds (11.00–78 µM). In the present data set, this represents the distance between the para-methoxy substituents at R<sub>1</sub> and R<sub>2</sub> of the aromatic rings in class B (Fig. 4J) and the distance between benzene ring attached at the linker region and the isoxazol ring in compound 37 of class C (IC<sub>50</sub> = 38 µM). Interestingly, the results of the TIP–TIP correlogram are further strengthened by our findings for the O–O correlogram that addition of para-methoxy groups to the aromatic moieties results in reduced biological activity. Interestingly, N1–TIP correlogram in Fig. 4A represents a distance of 18.00–18.40 Å between the molecular boundary depicted by the R<sub>1</sub> and R<sub>2</sub>

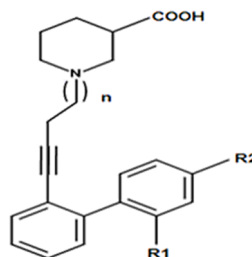
**Table 1** Summary of GRIND variables and their corresponding distances identified as highly correlated to biological activity ( $-\log IC_{50}$ ) of compounds.

Probes	Distances (Å)	Features	Impact	Comments
N1-N1	8.00-8.40	OH C=O	+	COOH group at meta position of piperidine, pyrrolidine, or azetidine ring has shown positive contribution towards hGAT1 inhibition activity ( $IC_{50}$ )
	14.00-14.40	C=O -O-	-	Carbonyl oxygen of the COOH group and the ether group present either in the linker region or in the bulky aromatic substituents has shown negative contribution towards the biological activity.
O-N1	5.60-6.00		+	Distance between protonated nitrogen of the piperidine, pyrrolidine, or azetidine ring and the COOH group
	10.40-10.80	COOH  OCH <sub>3</sub>	-	Protonated nitrogen of the piperidine ring and the methoxy substitution of the diaryl moieties
DRY-N1	10.40-10.80	Di/tri aryl moieties COOH	+	Distance between COOH group of piperidine, proline, pyrrolidine, or azetidine ring and bulky aromatic rings after linker chain
	6.40-6.80	Di/tri aryl moieties -O-	-	Distance between aromatic moieties and the ether group in the linker region
O-O	6.00-6.40	-O- X atom (any electronegative atom e.g., F, Cl <sup>-</sup> , O <sup>-</sup> , F <sup>-</sup> )	-	Depicts a distance between the ether group of hydrophilic chain and methoxy or fluoro group attached at para position of aromatic rings
TIP-TIP	12.40-12.80	OCH <sub>3</sub> OCH <sub>3</sub>	-	Distance between the methoxy substitutions on aromatic moieties attached at the linker region of hGAT1 antagonists

substitutions of the aromatic rings and the COOH group attached to the piperidine ring in the least active compounds. Thus, it may suggest the negative impact of  $R_1$  and  $R_2$  substitutions towards hGAT1 inhibitory potency as the importance of COOH group is already evident from N1-N1 and O-N1 variables. Overall, a brief summary of all the specific probes contributing towards the activity of hGAT1 antagonists is presented in [Table 1](#).

### External validation of the final GRIND model

To further demonstrate the predictive ability of the trained GRIND model, a recently published data set of 15 nipecotic acid derivatives possessing an alkyne type spacer (linker region) bridging the polar region at the aromatic rings, as shown in [Table 2](#), was used for external validation ([Lutz et al., 2017](#)).

**Table 2** External validation set of nipecotic acid derivatives of hGAT1 inhibitors.

Validation set compound # (VSC)	<i>n</i>	<i>R</i> <sub>1</sub>	<i>R</i> <sub>2</sub>	IC <sub>50</sub> μM	-log IC <sub>50</sub>	Predicted -log IC <sub>50</sub>	Residual value
VSC_1	1	H	H	0.10	1.00	0.24	0.75
VSC_2	1	F	H	0.07	1.12	0.33	0.78
VSC_3	1	CH <sub>3</sub>	CH <sub>3</sub>	0.20	0.68	-0.06	0.74
VSC_4	1	CH <sub>3</sub>	Cl	0.15	0.80	0.49	0.30
VSC_5	2	Cl	H	1.58	-0.20	0.33	-0.53
VSC_6	2	F	H	2.75	-0.44	0.26	-0.70
VSC_7	2	CH <sub>3</sub>	H	1.28	-0.11	0.13	-0.24
VSC_8	2	H	Cl	3.38	-0.53	-0.04	-0.48
VSC_9	2	Cl	Cl	0.93	0.03	-0.19	0.22
VSC_10	2	F	F	1.99	-0.30	-0.38	0.08
VSC_11	2	Cl	F	0.97	0.01	-0.06	0.07
VSC_12	2	CH <sub>3</sub>	Cl	0.97	0.01	0.20	-0.19
VSC_13	2	CH <sub>3</sub>	F	1.31	-0.12	0.19	-0.31
VSC_14	2	H	H	3.80	-0.58	0.37	-0.95
VSC_15	2	CH <sub>3</sub>	CH <sub>3</sub>	3.46	-0.54	0.40	-0.94

Overall, the IC<sub>50</sub> values of the data set range between 0.07 and 3.80 μM (Table 2). All the biological testing results (inhibitory potencies) were the mean of three independent experiments ± the standard error of the mean (Lutz *et al.*, 2017). Remarkably, all the compounds in the external validation set are well-predicted with *R*<sup>2</sup> value of 0.57 (Fig. 3, represented by triangles), and exhibiting a difference of less than one log unit between the experimental and predicted inhibitory values, as shown in Table 2.

### Homology modeling of hGAT1

Based on the alignment (representing 66% sequence similarity (Fig. S4); equivalent to 46% sequence identity) hGAT1 models in open to out conformation were constructed using dDAT as a template as explained in methodology section. The Ramachandran plot of the final selected model with best ERRAT value (81.28) in comparison to ERRAT values of rest of the models (range: 69.93–80.00) and Verify3D score (83.24%) has shown four residues in the outlier region, including F174 (EL2), N176 (EL2), R419 (TM9), and V528 (TM11). In order to further improve the model quality, final selected model was energy minimized via LigX using MMFF94x in MOE v2013.0802 (Halgren, 1996; Chemical Computing Group, 2013). After the energy minimization, the model was re-evaluated by PROCHECK and none of the residues were observed in the disallowed region (Fig. S5).

The Ramachandran plot displayed 93.2% of the residues of hGAT1 in most favored regions, 5.9% residues in additionally allowed regions, 0.9% residues in generously allowed regions, and 0.0% residues in disallowed regions. Similarly, the ERRAT (87.92) and Verify3D (85%) scores were also improved compared to the model before energy minimization. This further shows the reliability of the final model.

Briefly, ERRAT score provides information about the residues that contribute towards the lower percentage/score of the hGAT1 model (i.e., residues 165 to 180). This is may be because EL2 in hGAT1 contains a greater number of residues than in AaLeuT and dDAT. These may be the flanking residues of this loop. Furthermore, *Gether et al. (2006)* reported that binding of the ligand to the transporter in the open-to-out conformation results in the penetration of extracellular loop 4 (EL4) deep inside the hGAT1 binding site (i.e., TM1 residues), leading to the formation of a lid-type structure that seals the ligand into the hydrophobic core/region of the binding cavity. This confirms that the binding of the substrate to the transporter in its open-to-out form involves a major conformational change in EL4 (*Gether et al., 2006*). In the constructed hGAT1 model, EL4 penetration into the hydrophobic region of the binding cavity has resulted in the adjustment of bi- or tri-aromatic/ cyclic moieties of hGAT1 antagonists. Overall, the final model has 12 transmembrane (TM) segments, two Na<sup>+</sup> ions and one Cl<sup>-</sup> ion along with the bridging extracellular and intracellular loops. One side of the hydrophobic cavity around cyclic moieties is defined by the residues W68 (TM1b), Y139 (TM3), Y140 (TM3) and I143 (TM3) and the other by F294 (TM6a), S359 (EL4a), D451 (TM10), and S456 (TM10). The final structural model of hGAT1 in the open-to-out conformation, along with the two Na<sup>+</sup>, one Cl<sup>-</sup> and binding pocket residues are shown in [Fig. S6](#).

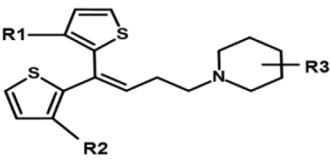
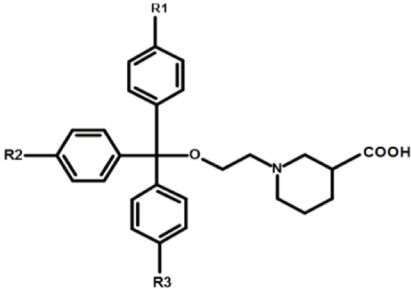
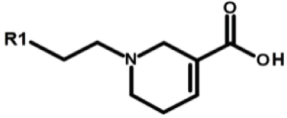
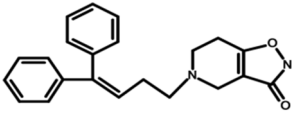
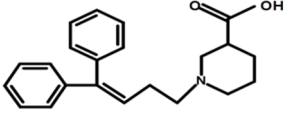
## Molecular docking of selected ligands in hGAT1

### Structure–activity relationship

On the basis of the SAR, four compounds each from classes A and B and five compounds from class C have been selected for further structure-based studies, as shown in [Table 3](#).

Briefly, **class A** includes N-diarylalkenyl piperidine COOH derivatives ([Table S1](#)) with a COOH group substituent at the ortho, meta or para position of the piperidine ring. COOH group in compounds **2** and **6** was R-configured however, stereochemistry of rest of the compounds in class A was not specified and thus, represent racemic mixtures. Compound **2** (Tiagabine, IC<sub>50</sub> = 0.049 μM), the only FDA approved antiepileptic drug, was selected for molecular docking to investigate its binding hypothesis and to compare it with rest of the analogs in class A. Compound **6** (IC<sub>50</sub> = 0.34 μM) was selected to evaluate the one order of magnitude decrease in its inhibitory potency compared to compound **2**, which may be due to the presence of bulky substituents (-CH<sub>2</sub>OC<sub>6</sub>H<sub>5</sub>) at R<sub>1</sub> and R<sub>2</sub> in compound **6** compared to methyl substituents at the same positions in compound **2**. Interestingly, compounds **8** and **15** have the same bulky substituents (-CH<sub>2</sub>OC<sub>6</sub>H<sub>5</sub>) at R<sub>1</sub> and R<sub>2</sub> as compound **6**; however, an approximate two-fold decrease in the biological activity has been observed, i.e., **6** (IC<sub>50</sub> = 0.34 μM) > **8** (IC<sub>50</sub> = 0.65 μM) > **15** (IC<sub>50</sub> = 1.5 μM) that can be correlated to the position (meta > ortho > para) of the COOH group on the piperidine ring. Briefly, compound **6** (IC<sub>50</sub> = 0.34 μM), which has the COOH

**Table 3** Selected compounds from classes A, B and C for experimental guided docking studies.

Common scaffolds					
Class A	Class B	Class C			
					
Compound #	Class scaffold	R <sub>1</sub>	R <sub>2</sub>	R <sub>3</sub>	IC <sub>50</sub> (μM)
2	A	-CH <sub>3</sub>	-CH <sub>3</sub>	m-COOH (R)	0.049
6	A	-CH <sub>2</sub> OC <sub>6</sub> H <sub>5</sub>	-CH <sub>2</sub> OC <sub>6</sub> H <sub>5</sub>	m-COOH (R)	0.34
8	A	-CH <sub>2</sub> OC <sub>6</sub> H <sub>5</sub>	-CH <sub>2</sub> OC <sub>6</sub> H <sub>5</sub>	o-COOH(R,S)	0.65
15	A	-CH <sub>2</sub> OC <sub>6</sub> H <sub>5</sub>	-CH <sub>2</sub> OC <sub>6</sub> H <sub>5</sub>	p-COOH(R,S)	1.5
14	B	H	H	H	1.4
27	B	H	-OCH <sub>3</sub>	H	6.9
36	B	-OCH <sub>3</sub>	-OCH <sub>3</sub>	-OCH <sub>3</sub>	30
40	B	-OCH <sub>3</sub>	-OCH <sub>3</sub>	H	43
1	C	-ON=C(C <sub>6</sub> H <sub>5</sub> ) <sub>2</sub>	-	-	0.040
3	C	-CH=C(C <sub>6</sub> H <sub>5</sub> ) <sub>2</sub>	-	-	0.20
4	C	-OCH(C <sub>6</sub> H <sub>5</sub> -m-CF <sub>3</sub> ) <sub>2</sub>	-	-	0.26
37	C				38
84	C				0.11

group at the meta position (m-COOH) of the piperidine ring, showed two-fold greater inhibitory potency against hGAT1 compared to compound **8** (IC<sub>50</sub> = 0.65 μM), which has a COOH group at the ortho position, and in turn showed two-fold greater activity as compared to compound **15** (IC<sub>50</sub> = 1.5 μM), which has a COOH group at the para position (p-COOH). Therefore, compounds **6**, **8** and **15** were also selected for docking within the binding cavity of hGAT1 to understand the binding hypothesis of the COOH group at the ortho, meta and para positions of the piperidine ring.

**Class B** of hGAT1 antagonists consists of ethyl trityl ether derivatives of nipecotic acid that possess a R- configured COOH group at the meta position (mCOOH) of the piperidine ring and R<sub>1</sub>, R<sub>2</sub> and R<sub>3</sub> methoxy substituents on the triphenylmethyl group, as shown in [Table S1](#). Compound **14** being the highly active in class B (IC<sub>50</sub> = 1.40 μM),



was selected for comparison with the rest of the data. Attachment of a para-methoxy group at R<sub>2</sub> in compound **27** results in a 5-fold decrease in the biological activity (6.9 μM) compared to compound **14**. Interestingly, para-methoxy substituents at R<sub>1</sub>, R<sub>2</sub> and R<sub>3</sub> in compound **36** (IC<sub>50</sub> = 30 μM) and at R<sub>1</sub> and R<sub>2</sub> in compound **40** (IC<sub>50</sub> = 43 μM) result in a decrease of approximately two orders of magnitude in the inhibitory potency against hGAT1 compared to compound **14**. This suggests that the decrease in the biological activity of compounds **27**, **36** and **40** compared to compound **14** is may be due to the presence of para-methoxy groups at R<sub>1</sub>, R<sub>2</sub> and R<sub>3</sub>, which might cause steric hindrance within the binding pocket or limit the access of the compounds to the hGAT1 binding pocket.

This is further validated by our findings from the GRIND model that para-methoxy substituents at aromatic moieties and the ether linker group at a mutual distance of 6.00–6.40 Å (O–O probes) have a negative effect on the hGAT1 inhibitory potency. Therefore, compounds **27**, **36** and **40** were also selected in addition to compound **14** for further molecular docking studies to probe the effect of para-methoxy substitutions on aromatic moieties on binding within the active site of hGAT1.

Compounds **1**, **3**, **4**, **37** and **84**, which are diaryl derivatives of nipecotic acid (all having racemic COOH groups with the exception of compound **37** as shown in [Table S1](#)) were selected from class **C** to elucidate the effect of the attachment of diaryl and the piperazine derivatives at the linker region on the biological activity of hGAT1 antagonists. Compound **1** (NNC-711), the 2-benzhydrylideneamino derivative of nipecotic acid, was selected as a reference ligand in the class since it is a known selective inhibitor of hGAT1 (IC<sub>50</sub> = 0.040 μM) ([Kragler, Höfner & Wanner, 2005](#)). However, replacement of the –C=NO– in compound **1** with –C=CH– and –CHO– in compounds **3** (SK&F-100330A) and **4** (CI-966) resulted in one order of magnitude decrease in the biological activities of compounds **3** (IC<sub>50</sub> = 0.20 μM) and **4** (IC<sub>50</sub> = 0.26 μM) compared to **1** (IC<sub>50</sub> = 0.040 μM). This decrease in biological activity has been correlated to an increase in the logP values, logP **4** (5.45) > logP **3** (4.19) > logP **1** (3.79), which may reflect the importance of polar groups in interactions within the binding pocket of hGAT1. As a result, compounds **1**, **3** and **4** were selected for further molecular docking and ligand–protein interaction profiling. Additionally, compound **84** was selected to compare its ligand–protein interaction profile with compound **3**. In compound **37**, replacement of the COOH group with 4,5,6,7-tetrahydroisoxazolo[4,5-c]pyridin-3-ol resulted in a three order of magnitude decrease in the inhibitory potency of the compound (IC<sub>50</sub> = 38 μM) compared to compound **1** (IC<sub>50</sub> = 0.040 μM). Therefore, compound **37** was selected to elucidate the effect of nipecotic acid on the inhibitory potency against hGAT1. This may point towards the importance of nipecotic acid in obtaining high inhibitory potency against hGAT1.

Briefly, all the selected compounds from class **A** (**2**, **6**, **8**, **15**), class **B** (**14**, **27**, **36**, **40**) and class **C** (**1**, **3**, **4**, **37**, **84**) were docked into the binding site of the hGAT1 model as explained in the methods section. To remove any biases in the docking protocol, 100 poses per ligand were generated using the GOLD score fitness function. However, the fitness function in Gold score is optimized for the prediction of binding positions rather

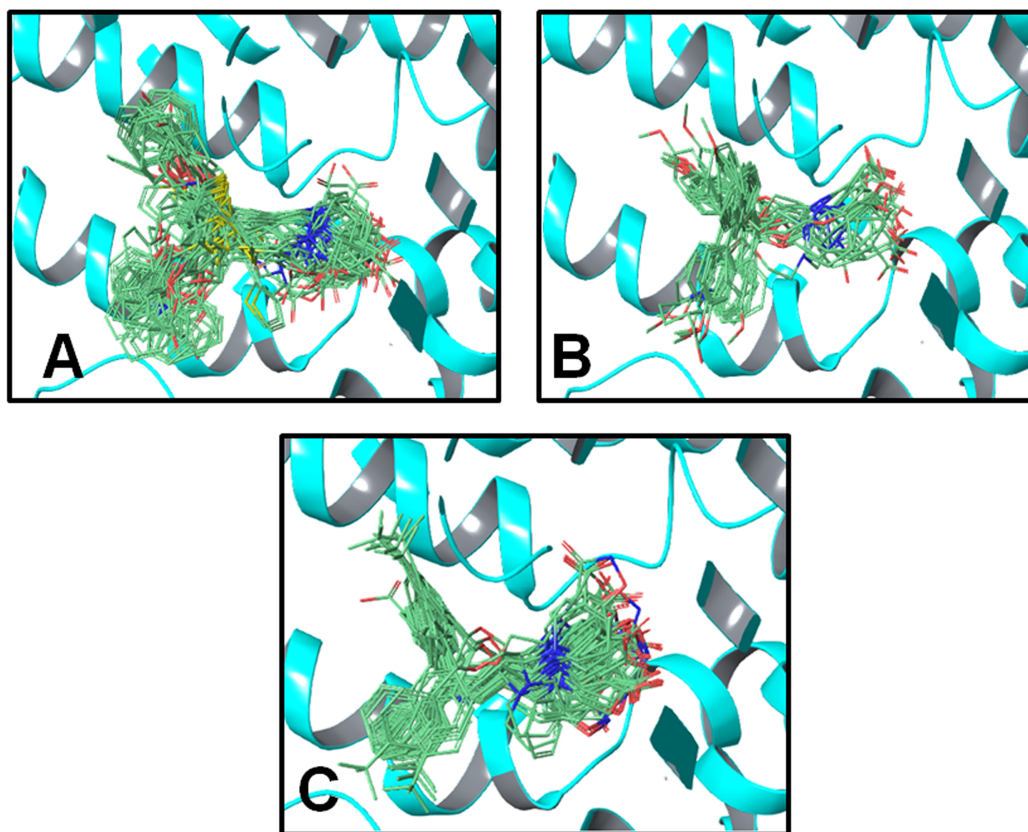


**Figure 5** Docking poses of clusters from classes A, B and C in hGAT1 binding pocket that contained maximum number of docked ligands from respective classes. (A) 14 clusters from class A containing three (2, 8, 15) out of four ligands. (B) 12 clusters from class B exhibiting three (14, 27, 36) out of four ligands. (C) Four clusters from class C possessing four (1, 3, 37, 84) out of five ligands.

Full-size DOI: 10.7717/peerj.6283/fig-5

than binding affinities (Jones, Willett & Glen, 1995) therefore, a poor correlation ( $R^2$ : 0.02) has been observed between biological activity ( $-\log IC_{50}$ ) and top scored pose of each ligand (Fig. S7; Table S4). Therefore, in order to remove any biases in the pose selection criteria, for the final ligand–protein interaction analysis, only one cluster exhibiting maximum docked ligands from each class was selected on the basis of the SAR and mutagenesis data, followed by energy minimization of the final ligand–protein complexes (Fig. S7; Table S4) (Halgren, 1996; Chemical Computing Group, 2013).

Briefly, a total number of 14 clusters of docking solutions of compounds in class A, 12 clusters of binding conformations of compounds in class B, and four clusters of binding solutions for the compounds in class C have been identified that contained the maximum number of docked ligands. Briefly, all 14 clusters of class A contained three (2, 8, 15) out of four docked ligands, 12 clusters of class B also contained three (14, 27, 36) out of four docked ligands and four clusters of class C contained four (1, 3, 37, 84) out of five docked ligands as shown in Fig. 5.

The binding position of all the 14 clusters in class A was approximately the same. However, the binding conformations of the docking solutions in each cluster were

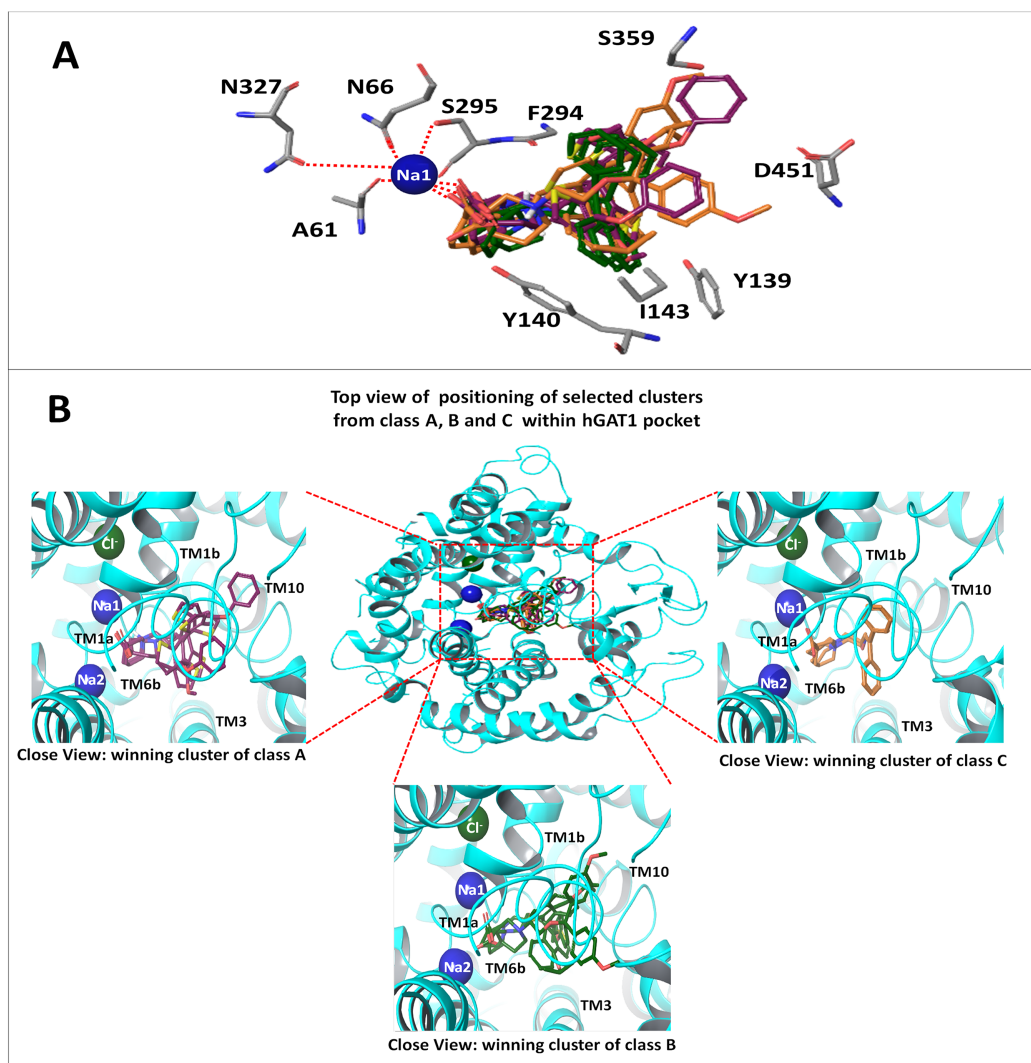


**Figure 6** Winning clusters obtained from docking of hGAT1 antagonists. (A) Final docking poses of hGAT1 antagonists from classes A, B and C. Positioning of di- or tri-aromatic rings represent the hydrophobic areas and charged piperidine ring represent the polar region in the binding pocket of hGAT1. (B) Binding positions of winning clusters of classes A, B and C in hGAT1 binding pocket along with Na1, Na2 (blue spheres) and a Cl<sup>-</sup> (green sphere) ion.

Full-size DOI: 10.7717/peerj.6283/fig-6

different. Therefore, the interaction patterns of all 14 clusters of class A were explored and only one cluster that is strengthened by the SAR and mutagenesis data was selected for the final ligand–protein interaction analysis. A similar selection procedure was repeated for the 12 clusters of binding solutions for the selected compounds in class B and the four clusters of binding poses for the selected compounds in class C. Sodium ion (represented by Na1) was involved in interactions with the COOH attached to the piperidine ring in all three classes, as well as with the amino acid residues A61, N66, S295, and N327, as shown in Fig. 6A.

Overall, the winning cluster of class A showed interactions with TM segments 1a, 1b, 6a, 6b and 10 (Fig. 6B). It has been observed that the carbonyl group at the meta position

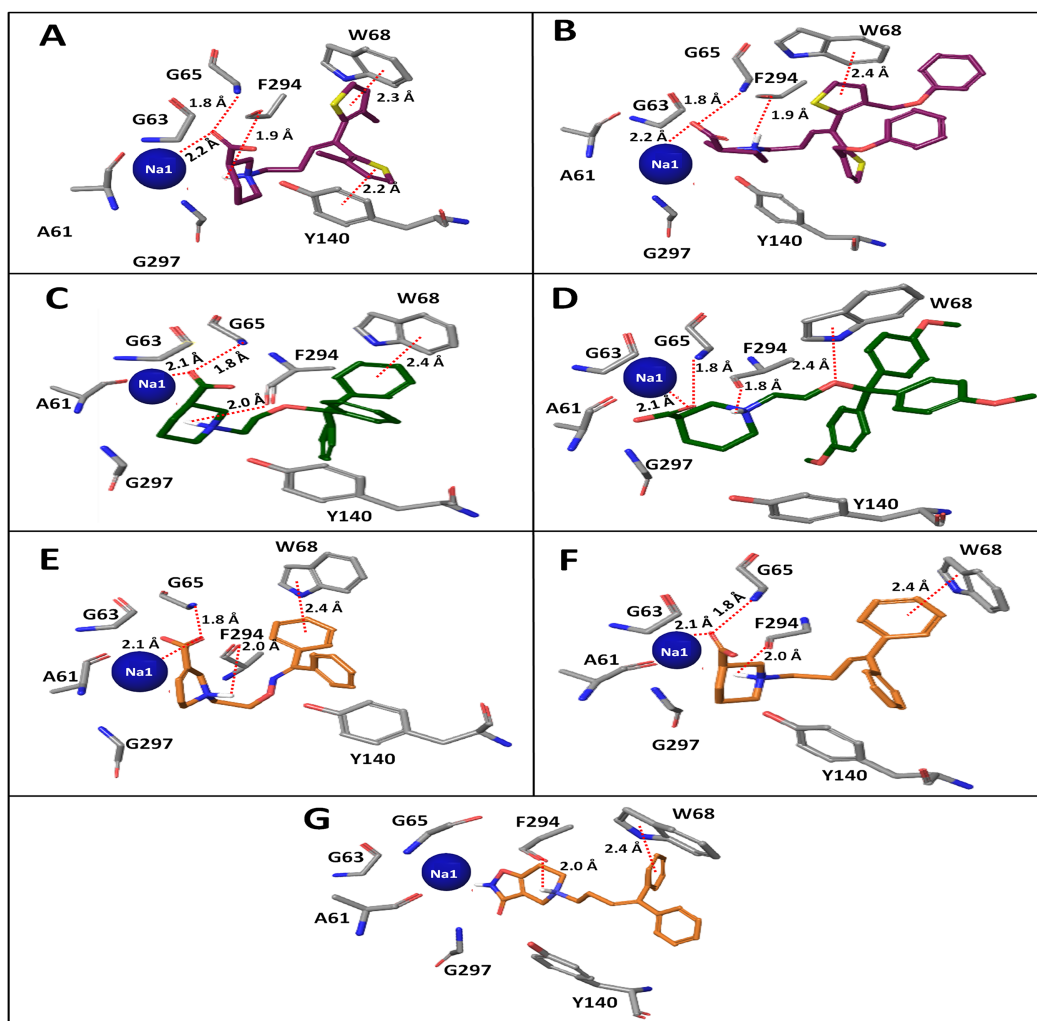


**Figure 7** Interaction pattern of binding solutions of classes A, B and C in hGAT1 model. Ligand–protein interactions of (A) compound 2 and (B) compound 8 of class A. Interactions pattern of (C) compound 14 and (D) compound 36 of class B. Binding poses of (E) compound 1, (F) compound 3 and (G) compound 37 of class C. [Full-size !\[\]\(5f471a71b78d7676bc356df190b88ab4\_img.jpg\) DOI: 10.7717/peerj.6283/fig-7](https://doi.org/10.7717/peerj.6283/fig-7)

of the piperidine ring in compound 2 shows a strong hydrogen bonding interaction with the –NH group of G65, whereas the thiophene rings of the common scaffold shows a  $\pi$ – $\pi$  interaction with Y140 at TM3 and W68 at TM1b (Fig. 7A). Additionally, F294 of TM6a shows a strong hydrogen bonding interaction with the protonated nitrogen of the piperidine ring. In compounds 8 and 15 hydrogen bonding is observed between the –NH group of G65 and the OH group of the COOH, as shown in Fig. 7B. Thus, the one order of magnitude decrease in the inhibitory potency of compounds 8 and 15 compared to compound 2 may be attributed to a decrease in the hydrogen bonding strength due to a shift in the position of the hydrogen bond from the carbonyl group (in compound 2) to the hydroxyl group (in compounds 8 and 15). The COOH flipping is might be due to the shift of the COOH group from the meta position to the ortho and para positions of the piperidine ring in compounds 8 and 15, respectively.

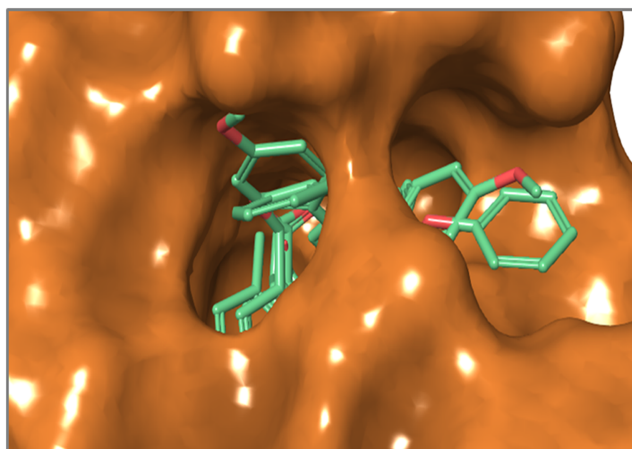


**Figure 8** Outward projection of bulky substitutions on aromatic moieties of antagonists of class A and B from the hGAT1 binding pocket. [Full-size !\[\]\(b345a1c4255362eec3746050dd71ccac\_img.jpg\) DOI: 10.7717/peerj.6283/fig-8](https://doi.org/10.7717/peerj.6283/fig-8)

Additionally, the ligand–protein interaction pattern of the final docking poses of compounds **8** and **15** reveals that bulky substituents at the R<sub>1</sub> and R<sub>2</sub> positions are more exposed to the extracellular environment (Fig. 8). This disrupts the  $\pi$ - $\pi$  stacking between the phenyl ring of Y140 and the thiophene ring associated with R<sub>1</sub> in compounds **8** and **15**, which was present in compound **2**. However, the  $\pi$ - $\pi$  interaction between the thiophene ring of the common scaffold of class A and the indole ring of W68 at TM1b and the hydrogen bonding interaction between the protonated nitrogen of the piperidine ring and F294 at TM6a remained intact, as shown in Fig. 7B. Therefore, this shows that the bulky substituents on the thiophene rings in compounds **8** and **15** result in a loss of the interaction with Y140, which is known to be critical for the transport activity of GATs (Bismuth, Kavanaugh & Kanner, 1997). These results agree with our SAR data showing that the attachment of bulky groups at the R<sub>1</sub> and R<sub>2</sub> positions in class A, together with the positioning of the COOH on the piperidine ring, may affect the inhibitory potency against hGAT1. Overall, the amino acid residues G65, W68, Y140 and F294 are involved in interactions with the N-diarylalkenyl piperidine COOH derivatives within the hGAT1 binding cavity.

Similarly, out of 12 clusters of binding solutions of compounds in class B, only one cluster (Fig. 6B), which contains the binding poses of compounds **14**, **27** and **36**, followed the SAR pattern in their ligand–protein interaction profile. However, the rest of the clusters shared similar overall binding positions within the binding pocket of hGAT1. As all the compounds in class B have a meta-COOH and a protonated nitrogen in piperidine ring, their binding solutions showed a very similar pattern of hydrogen bonding interactions with the residues G65 and F294 and with Na1, as shown by compound **2** in class A. However, the benzene ring of the common scaffold in compound **14** shows a  $\pi$ - $\pi$  interaction with the indole ring of W68 at TM1b (Fig. 7C). Additionally, both compounds **27** and **36** (Fig. 7D) shows hydrogen bonding interactions between the ether group in the linker region and the pyrrole ring of W68. Similar to the compounds **8** and **15** in class A, the methoxy substitutions on the aromatic moieties in

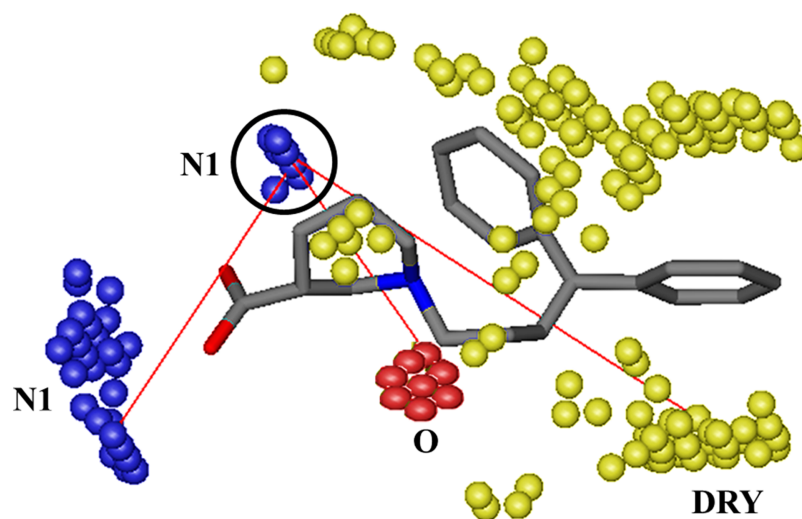


**Figure 9** Important hotspots regions for the high inhibitory potency of hGAT1 inhibitors. One hydrogen bond acceptor contour (N1) at a distance of 8.00–8.40 Å from second hydrogen bond acceptor (N1) group, at a distance of 5.60–6.00 Å from a hydrogen bond donor (O) and at a distance of 10.40–10.80 Å from a hydrophobic (DRY) group. [Full-size](#) DOI: 10.7717/peerj.6283/fig-9

compounds **27** and **36** projected out of the hGAT1 binding pocket (Fig. 8). They may require a large space in the cavity compared to compound **14**, and as a result showed no interaction with the residues in the hGAT1 binding pocket.

Similar to the selected clusters of class A and B, the final cluster of class C followed the SAR and mutagenesis data. The final binding solutions for class C contain compounds **1**, **3**, **37** and **84**, which are located in the vicinity of TM1a, TM1b, TM4, TM6a and TM6b (Fig. 6B). The selected compounds in class C show a  $\pi$ - $\pi$  interaction with W68, followed by a similar hydrogen bonding interaction pattern at the protonated nitrogen atom (NH–O=C–F294) and at the COOH group (C=O–HN–G65) (Figs. 7E and 7F) (ligplot shown in Fig. S8) as that discussed for classes A (compound **2**) and B. However, compound **37** is an exception in which the COOH is replaced with a five membered isoxazol ring. The residues surrounding Na1 are similar in the case of compound **37**, as shown in Fig. 7G. Thus, the two to three orders of magnitude decrease in the inhibitory potency of compound **37** compared to its congeners is might be due to lack of COOH group and its associated interactions within the hGAT1 pocket.

## DISCUSSION

In present study, we demonstrated the importance of COOH group towards hGAT1 inhibition. Our final GRIND model mapped the distances of important pharmacophoric features of the ligands, including one hydrogen bond acceptor (N1), one hydrogen bond donor (O) and one hydrophobic (Dry) probe from the COOH group at meta- position of the piperidine ring as shown in Fig. 9 which reflect that COOH group at meta position of the piperidine ring may provide an important interaction point within the binding cavity of hGAT1.

Figure 9 is further validated by our SAR and docking protocol, where all three classes A, B and C showed interactions between the protonated nitrogen atom and F294 and between the COOH group and G65. The effect of the COOH group, as well as the protonated nitrogen atom, on the inhibitory potency of hGAT1 modulators has been previously demonstrated by various authors (Zhao *et al.*, 2005; Fülep *et al.*, 2006; Kragler, Höfner & Wanner, 2008; Pizzi *et al.*, 2011). Therefore, three orders of magnitude decrease in inhibitory potency of compound 37 as compared to compound 1 is may be due to absence of COOH group in its chemical scaffold.

Furthermore, COOH groups at the meta position of docked antagonists (class A; compound 2 and class B) has been observed in the equatorial conformation with respect to Na1 in the hGAT1 model (Fig. 6A). Thus, it suggests that the meta positioning of the equatorial COOH group is more favorable for obtaining more potent hGAT1 antagonists compared to equatorial ortho or para COOH positioning. This observation agrees with previous studies by Skovstrup *et al.* (2010) and Jurik *et al.* (2015), who demonstrated that the R-configured COOH group in an axial conformation with respect to Na1 is involved in intramolecular hydrogen bonding with the protonated nitrogen of the piperidine ring. Thus, attachment of bulky groups (i.e., COOH) in an axial configuration with respect to Na1 is not favorable (Jurik *et al.*, 2015). Previously, various authors proposed R-configured COOH group in hGAT1 antagonists as favorable binding conformation (Borden *et al.*, 1994; Wermuth, 2008; Schmidt, Höfner & Wanner, 2017). However, in present study the stereochemical effect of hGAT1 antagonists in ligand protein interaction could not be considered due to lack of complete stereoisomers data.

Our results also demonstrate the negative impact of methoxy substitutions at R<sub>1</sub>, R<sub>2</sub> or R<sub>3</sub> positions of di- or tri-aryl rings and the ether linker group towards GAT1 inhibition. We hypothesize that 7-fold decrease in the biological activity of compound 27 (IC<sub>50</sub> = 6.9 μM) and one order of magnitude decrease in the biological activity of compound 36 (IC<sub>50</sub> = 30 μM) as compared to compound 14 (IC<sub>50</sub> = 1.4 μM) is may be due to attachment of methoxy groups at R<sub>1</sub>, R<sub>2</sub> or R<sub>3</sub>. This is supported by the O–O (Figs. 4H and 4I) and TIP–TIP correlograms (Fig. 4J) of the final GRIND model. Both distance features (O–O and TIP–TIP) are arising from methoxy or ether linker substituents and show a negative effect on the inhibitory potency against hGAT1. In compounds 27, 36 and 40 of class B, these map the distance between the ether in the linker region and the para-methoxy groups at the R<sub>2</sub> position. Hence the biological activity values of compounds 27, 36 and 40 (6.9 μM, 30 μM and 43 μM) are significantly reduced compared to compound 14 (1.4 μM), which lacks electronegative atom substituents at the R<sub>1</sub>, R<sub>2</sub> and R<sub>3</sub> positions. Additionally, two orders of magnitude decrease in the inhibitory potency of compounds in class B compared to compounds in class A is may be attributed to the presence of the para-methoxy group in the common scaffold for class B compared to common scaffold of class A. This is further strengthened by a study by Pizzi *et al.* (2011), who studied the effect of ortho, meta and para substitutions on 4,4-diphenylbut-3-enyl derivatives and observed that biological activity against hGAT1 reduces with the substitution of methyl, chloride, fluoride and bromide at the ortho position of the di-aryl

rings. This is also strengthened by the ligand protein interaction analysis of the final docking poses of compounds of classes A, B and C which elucidate that the bulky substitutions at R<sub>1</sub> and R<sub>2</sub> positions of di- or tri-aryl rings are projected out of the binding cavity, exposed to the extracellular environment and thus, are not well fitted within the binding cavity of hGAT1.

Overall, the ligand-protein interactions profile of selected hGAT1 inhibitors of classes A, B and C showed significant role of G65, W68, Y140 and F294 amino acid residues within the hGAT1 binding pocket. Previously, *Baglo et al. (2013)*, revealed hydrogen bonding and  $\pi$ - $\pi$  stacking with G65, N66, Y140, F294 and S295 by docking substrate-like small molecules (i.e., 5-aminolevulinic acid (ALA), and methyl ester of ALA (MAL)) in the hGAT1 model. Additionally, various structure-based studies identified the binding hypothesis of Tiagabine and demonstrated the role of the amino acid residues W68, Y139, Y140, I143, F294, A358 and S359 in the formation of hydrophobic pockets in hGAT1 (*Skovstrup et al., 2010; Jurik et al., 2015*). Overall, the ligand-protein interaction profiles of the final binding solutions of hGAT1 inhibitors from classes A, B and C were compared to the already known interaction patterns of other classes of respective modulators, as shown in [Fig. S9](#). It is evident from [Fig. S9](#) that the N-diarylalkenyl piperidine derivatives of class A show an overlap with all of the residues already reported in the literature except D451. Similarly, the interaction profile of class B agrees with that of class A, with the exception of S456. The nipecotic acid derivatives in class C completely agree with the literature, thus further validating the binding hypothesis of selected hGAT1 antagonists.

On the basis of these findings, further analyses will focus on virtual screening followed by activity and ADME profiling of subsequent hits and optimization of respective chemical scaffolds structures to identify new arsenal of hGAT1 antagonists with improved efficacy and better ADME properties.

## CONCLUSION

The current study probes the 3D structural features and binding hypothesis of hGAT1 inhibitors in the binding pocket of an in-house homology model of hGAT1 in the open-to-out conformation. Overall, our GRIND model illustrated the importance of two hydrogen bond acceptor groups at mutual distance of 8.00–8.40 Å, one hydrogen bond donor and one hydrophobic group at distance of 5.60–6.00 Å and 10.40–10.80 Å, respectively from one of the hydrogen bond acceptors for achieving high biological activity against hGAT1. However, the docking studies of nipecotic acid and N-diarylalkenyl piperidine analogs in the binding pocket of the hGAT1 model emphasized that the protonated nitrogen atom is oriented towards the extracellular side of the binding pocket due to the attachment of large hydrophobic moieties. In addition, Na1 and the residues G65, W68, Y140 and F294 in the binding pocket showed dominant interactions with the COOH group, aromatic moieties and the protonated nitrogen atom in the hGAT1 antagonists, respectively, that are important for achieving high activity against hGAT1. Both the GRIND model and the docking studies revealed that a meta-COOH group attached to the piperidine ring of hGAT1 antagonists



is more favorable for interactions compared to an ortho or para substituted COOH group. Moreover, the hydrogen bonding and the specific shape/orientation of the antagonists were found to be significant for achieving highly potent hGAT1 antagonists. Overall, we anticipate that the current study may assist the development of more effective antagonists for the treatment of epilepsy and other associated neurological disorders.

## ADDITIONAL INFORMATION AND DECLARATIONS

### Funding

Support was provided by HEC 'Indigenous Ph.D. Fellowship for 5,000 scholars' Phase-II, Batch-I, 2012. The funders had no role in study design, data collection and analysis, decision to publish, or preparation of the manuscript.

### Grant Disclosure

The following grant information was disclosed by the authors:  
HEC 'Indigenous Ph.D. Fellowship for 5,000 scholars' Phase-II, Batch-I, 2012.

### Competing Interests

The authors declare that the research was conducted in the absence of any commercial or financial relationships that could be construed as a potential conflict of interest.

### Author Contributions

- Sadia Zafar performed the experiments, analyzed the data, contributed reagents/materials/analysis tools, prepared figures and/or tables, authored or reviewed drafts of the paper.
- Ishrat Jabeen conceived and designed the experiments, analyzed the data, contributed reagents/materials/analysis tools, authored or reviewed drafts of the paper, approved the final draft.

### Data Availability

The following information was supplied regarding data availability:

The data used in this work is available in the [Supplemental Files](#).

### Supplemental Information

Supplemental information for this article can be found online at <http://dx.doi.org/10.7717/peerj.6283#supplemental-information>.

## REFERENCES

- Alexander SPH, Mathie A, Peters JA. 2007. Cell-surface transmitter transporters. *British Journal of Pharmacology* 150(S1):S135–S142 DOI 10.1038/sj.bjp.0707207.
- Alexander SPH, Mathie A, Peters JA. 2011. Guide to receptors and channels (GRAC), 5th edition. *British Journal of Pharmacology* 164:S1–S2 DOI 10.1111/j.1476-5381.2011.01649\_1.x.

- Alexander DLJ, Tropsha A, Winkler DA. 2015.** Beware of R 2: simple, unambiguous assessment of the prediction accuracy of QSAR and QSPR models. *Journal of Chemical Information and Modeling* 55(7):1316–1322 DOI 10.1021/acs.jcim.5b00206.
- Anderson CM, Kidd PD, Eskandari S. 2010.** GATMD:  $\gamma$ -aminobutyric acid transporter mutagenesis database. *Database* 2010:baq028 DOI 10.1093/database/baq028.
- Andersen KE, Sørensen JL, Lau J, Lundt BF, Petersen H, Huusfeldt PO, Suzdak PD, Swedberg MD. 2001.** Synthesis of novel  $\gamma$ -aminobutyric acid (GABA) uptake inhibitors. 5. 1 preparation and structure-activity studies of tricyclic analogues of known GABA uptake inhibitors. *Journal of Medicinal Chemistry* 44(13):2152–2163 DOI 10.1021/jm990513k.
- Baglo Y, Gabrielsen M, Sylte I, Gederaas OA. 2013.** Homology modeling of human  $\gamma$ -butyric acid transporters and the binding of pro-drugs 5-aminolevulinic acid and methyl aminolevulinic acid used in photodynamic therapy. *PLOS ONE* 8(6):e65200 DOI 10.1371/journal.pone.0065200.
- Baroni M, Costantino G, Cruciani G, Riganelli D, Valigi R, Clementi S. 1993.** Generating optimal linear PLS estimations (GOLPE): an advanced chemometric tool for handling 3DQSAR problems. *Quantitative Structure-Activity Relationships* 12(1):9–20 DOI 10.1002/qsar.19930120103.
- Bicho A, Grewer C. 2005.** Rapid substrate-induced charge movements of the GABA transporter GAT1. *Biophysical Journal* 89(1):211–231 DOI 10.1529/biophysj.105.061002.
- Bismuth Y, Kavanaugh MP, Kanner BI. 1997.** Tyrosine 140 of the  $\gamma$ -aminobutyric acid transporter GAT-1 plays a critical role in neurotransmitter recognition. *Journal of Biological Chemistry* 272(26):16096–16102 DOI 10.1074/jbc.272.26.16096.
- Borden LA, Dhar TGM, Smith KE, Weinshank RL, Branchek TA, Gluchowski C. 1994.** Tiagabine, SK&F 89976-A, CI-966, and NNC-711 are selective for the cloned GABA transporter GAT-1. *European Journal of Pharmacology: Molecular Pharmacology* 269(2):219–224 DOI 10.1016/0922-4106(94)90089-2.
- Bouanich J-P. 1992.** Site-site Lennard-Jones potential parameters for N<sub>2</sub>, O<sub>2</sub>, H<sub>2</sub>, CO and CO<sub>2</sub>. *Journal of Quantitative Spectroscopy and Radiative Transfer* 47(4):243–250 DOI 10.1016/0022-4073(92)90142-Q.
- Bowie JU, Luthy R, Eisenberg D. 1991.** A method to identify protein sequences that fold into a known three-dimensional structure. *Science* 253(5016):164–170 DOI 10.1126/science.1853201.
- Calapai G, Crupi A, Firenzuoli F, Inferred G, Squadrito F, Parisi A, De Sarro G, Caputi A. 2001.** Serotonin, norepinephrine and dopamine involvement in the antidepressant action of hypericum perforatum. *Pharmacopsychiatry* 34(2):45–49 DOI 10.1055/s-2001-15180.
- Carvill GL, McMahon JM, Schneider A, Zemel M, Myers CT, Saykally J, Nguyen J, Robbiano A, Zara F, Specchio N, Mecarelli O, Smith RL, Leventer RJ, Møller RS, Nikanorova M, Dimova P, Jordanova A, Petrou S, Helbig I, Striano P, Weckhuysen S, Berkovic SF, Scheffer IE, Mefford HC. 2015.** Mutations in the GABA transporter SLC6A1 cause epilepsy with myoclonic-atonic seizures. *American Journal of Human Genetics* 96(5):808–815 DOI 10.1016/j.ajhg.2015.02.016.
- Chemical Computing Group. 2013.** *Molecular Operating Environment (MOE)*. Version 2013.0802. Montreal: Chemical Computing Group.
- Clausen RP, Madsen K, Larsson OM, Frølund B, Krogsgaard-Larsen P, Schousboe A. 2006.** Structure-activity relationship and pharmacology of  $\gamma$ -aminobutyric acid (GABA) transport inhibitors. *Advances in Pharmacology* 54:265–284 DOI 10.1016/S1054-3589(06)54011-6.
- Clausen RP, Moltzen EK, Perregaard J, Lenz SM, Sanchez C, Falch E, Frølund B, Bolvig T, Sarup A, Larsson OM, Schousboe A, Krogsgaard-Larsen P. 2005.** Selective inhibitors of

- GABA uptake: synthesis and molecular pharmacology of 4-N-methylamino-4,5,6,7-tetrahydrobenzo[d]isoxazol-3-ol analogues. *Bioorganic & Medicinal Chemistry* **13**(3):895–908 DOI [10.1016/j.bmc.2004.10.029](https://doi.org/10.1016/j.bmc.2004.10.029).
- Colovos C, Yeates TO. 1993.** Verification of protein structures: patterns of nonbonded atomic interactions. *Protein Science* **2**(9):1511–1519 DOI [10.1002/pro.5560020916](https://doi.org/10.1002/pro.5560020916).
- Conti F, Melone M, De Biasi S, Minelli A, Brecha NC, Ducati A. 1998.** Neuronal and glial localization of GAT-1, a high-affinity  $\gamma$ -aminobutyric acid plasma membrane transporter, in human cerebral cortex: With a note on its distribution in monkey cortex. *Journal of Comparative Neurology* **396**:51–63 DOI [10.1002/\(SICI\)1096-9861\(19980622\)396:1<51::AID-CNE5>3.0.CO;2-H](https://doi.org/10.1002/(SICI)1096-9861(19980622)396:1<51::AID-CNE5>3.0.CO;2-H).
- Conti F, Zuccarello LV, Barbaresi P, Minelli A, Brecha NC, Melone M. 1999.** Neuronal, glial, and epithelial localization of  $\gamma$ -aminobutyric acid transporter 2, a high-affinity  $\gamma$ -aminobutyric acid plasma membrane transporter, in the cerebral cortex and neighboring structures. *Journal of Comparative Neurology* **409**:482–494 DOI [10.1002/\(SICI\)1096-9861\(19990705\)409:3<482::AID-CNE11>3.0.CO;2-O](https://doi.org/10.1002/(SICI)1096-9861(19990705)409:3<482::AID-CNE11>3.0.CO;2-O).
- Dalby NO. 2000.** GABA-level increasing and anticonvulsant effects of three different GABA uptake inhibitors. *Neuropharmacology* **39**(12):2399–2407 DOI [10.1016/S0028-3908\(00\)00075-7](https://doi.org/10.1016/S0028-3908(00)00075-7).
- Dhar TGM, Borden LA, Tyagarajan S, Smith KE, Branchek TA, Weinshank RL, Gluchowski C. 1994.** Design, synthesis and evaluation of substituted triaryl nipecotic acid derivatives as GABA uptake inhibitors: identification of a ligand with moderate affinity and selectivity for the cloned human GABA transporter GAT-3. *Journal of Medicinal Chemistry* **37**(15):2334–2342 DOI [10.1021/jm00041a012](https://doi.org/10.1021/jm00041a012).
- Durán Á, Martínez GC, Pastor M. 2008.** Development and validation of AMANDA, a new algorithm for selecting highly relevant regions in molecular interaction fields. *Journal of Chemical Information and Modeling* **48**(9):1813–1823 DOI [10.1021/ci800037t](https://doi.org/10.1021/ci800037t).
- Durán Á, Pastor M. 2011.** An advanced tool for computing and handling GRid-INdependent. *Descriptors User Manual Version*. Vol. 1.
- Elisseeff A, Pontil M. 2003.** Leave-one-out error and stability of learning algorithms with applications. *NATO Science Series Sub Series iii Computer and Systems Sciences*. Vol. 190. Amsterdam: IOS press, 111–130.
- Faust MR, Höfner G, Pabel J, Wanner KT. 2010.** Azetidine derivatives as novel  $\gamma$ -aminobutyric acid uptake inhibitors: Synthesis, biological evaluation, and structure–activity relationship. *European Journal of Medicinal Chemistry* **45**(6):2453–2466 DOI [10.1016/j.ejmech.2010.02.029](https://doi.org/10.1016/j.ejmech.2010.02.029).
- Fülep GH, Hoesl CE, Höfner G, Wanner KT. 2006.** New highly potent GABA uptake inhibitors selective for GAT-1 and GAT-3 derived from (R)- and (S)-proline and homologous pyrrolidine-2-alkanoic acids. *European Journal of Medicinal Chemistry* **41**(7):809–824 DOI [10.1016/j.ejmech.2006.01.019](https://doi.org/10.1016/j.ejmech.2006.01.019).
- Gether U, Andersen PH, Larsson OM, Schousboe A. 2006.** Neurotransmitter transporters: molecular function of important drug targets. *Trends in Pharmacological Sciences* **27**(7):375–383 DOI [10.1016/j.tips.2006.05.003](https://doi.org/10.1016/j.tips.2006.05.003).
- Gillet VJ. 2011.** Diversity selection algorithms. *Wiley Interdisciplinary Reviews: Computational Molecular Science* **1**(4):580–589 DOI [10.1002/wcms.33](https://doi.org/10.1002/wcms.33).
- Halgren TA. 1996.** Merck molecular force field. I. Basis, form, scope, parameterization, and performance of MMFF94. *Journal of Computational Chemistry* **17**:490–519 DOI [10.1002/\(SICI\)1096-987X\(199604\)17:5/6<490::AID-JCC1>3.0.CO;2-P](https://doi.org/10.1002/(SICI)1096-987X(199604)17:5/6<490::AID-JCC1>3.0.CO;2-P).
- Hauke TJ, Wein T, Höfner G, Wanner KT. 2018.** Novel allosteric ligands of  $\gamma$ -aminobutyric acid transporter 1 (GAT1) by MS based screening of pseudostatic hydrazone libraries. *Journal of Medicinal Chemistry* **61**(22):10310–10332 DOI [10.1021/acs.jmedchem.8b01602](https://doi.org/10.1021/acs.jmedchem.8b01602).

- Hellenbrand T, Höfner G, Wein T, Wanner KT. 2016.** Synthesis of 4-substituted nipecotic acid derivatives and their evaluation as potential GABA uptake inhibitors. *Bioorganic & Medicinal Chemistry* **24(9)**:2072–2096 DOI [10.1016/j.bmc.2016.03.038](https://doi.org/10.1016/j.bmc.2016.03.038).
- Heng JI-T, Moonen G, Nguyen L. 2007.** REVIEW ARTICLE: Neurotransmitters regulate cell migration in the telencephalon. *European Journal of Neuroscience* **26(3)**:537–546 DOI [10.1111/j.1460-9568.2007.05694.x](https://doi.org/10.1111/j.1460-9568.2007.05694.x).
- Hirayama BA, Díez-Sampedro A, Wright EM. 2001.** Common mechanisms of inhibition for the Na<sup>+</sup>/glucose (hSGLT1) and Na<sup>+</sup>/Cl<sup>-</sup>/GABA (hGAT1) cotransporters. *British Journal of Pharmacology* **134(3)**:484–495 DOI [10.1038/sj.bjp.0704274](https://doi.org/10.1038/sj.bjp.0704274).
- Ho BK, Brasseur R. 2005.** The Ramachandran plots of glycine and pre-proline. *BMC Structural Biology* **5(1)**:14 DOI [10.1186/1472-6807-5-14](https://doi.org/10.1186/1472-6807-5-14).
- Jin X-T, Galvan A, Wichmann T, Smith Y. 2011.** localization and function of GABA transporters GAT-1 and GAT-3 in the basal ganglia. *Frontiers in System Neuroscience* **5(63)**:1–10 DOI [10.3389/fnsys.2011.00063](https://doi.org/10.3389/fnsys.2011.00063).
- Jones G, Willett P, Glen RC. 1995.** Molecular recognition of receptor sites using a genetic algorithm with a description of desolvation. *Journal of Molecular Biology* **245(1)**:43–53 DOI [10.1016/S0022-2836\(95\)80037-9](https://doi.org/10.1016/S0022-2836(95)80037-9).
- Jurik A, Reicherstorfer R, Zdrzil B, Ecker GF. 2013.** Classification of high-activity tiagabine analogs by binary QSAR modeling. *Molecular Informatics* **32(5-6)**:415–419 DOI [10.1002/minf.201300020](https://doi.org/10.1002/minf.201300020).
- Jurik A, Zdrzil B, Holy M, Stockner T, Sitte HH, Ecker GF. 2015.** A binding mode hypothesis of tiagabine confirms liothyronine effect on  $\gamma$ -aminobutyric acid transporter 1 (GAT1). *Journal of Medicinal Chemistry* **58(5)**:2149–2158 DOI [10.1021/jm5015428](https://doi.org/10.1021/jm5015428).
- Kragler A, Höfner G, Wanner KT. 2005.** Novel parent structures for inhibitors of the murine GABA transporters mGAT3 and mGAT4. *European Journal of Pharmacology* **519(1-2)**:43–47 DOI [10.1016/j.ejphar.2005.06.053](https://doi.org/10.1016/j.ejphar.2005.06.053).
- Kragler A, Höfner G, Wanner KT. 2008.** Synthesis and biological evaluation of aminomethylphenol derivatives as inhibitors of the murine GABA transporters mGAT1-mGAT4. *European Journal of Medicinal Chemistry* **43(11)**:2404–2411 DOI [10.1016/j.ejmech.2008.01.005](https://doi.org/10.1016/j.ejmech.2008.01.005).
- Labute P. 2008.** The generalized Born/volume integral implicit solvent model: estimation of the free energy of hydration using London dispersion instead of atomic surface area. *Journal of Computational Chemistry* **29(10)**:1693–1698 DOI [10.1002/jcc.20933](https://doi.org/10.1002/jcc.20933).
- Lennard-Jones JE. 1931.** Cohesion. *Proceedings of the Physical Society* **43(5)**:461–482 DOI [10.1088/0959-5309/43/5/301](https://doi.org/10.1088/0959-5309/43/5/301).
- Lovell SC, Davis IW, Arendall WB III, de Bakker PIW, Word JM, Prisant MG, Richardson JS, Richardson DC. 2003.** Structure validation by C $\alpha$  geometry:  $\phi$ ,  $\psi$  and C $\beta$  deviation. *Proteins: Structure, Function, and Bioinformatics* **50(3)**:437–450 DOI [10.1002/prot.10286](https://doi.org/10.1002/prot.10286).
- Lüthy R, Bowie JU, Eisenberg D. 1992.** Assessment of protein models with three-dimensional profiles. *Nature* **356(6364)**:83–85 DOI [10.1038/356083a0](https://doi.org/10.1038/356083a0).
- Lutz T, Wein T, Höfner G, Pabel J, Eder M, Dine J, Wanner KT. 2018.** Development of new photoswitchable azobenzene based  $\gamma$ -aminobutyric acid (GABA) uptake inhibitors with distinctly enhanced potency upon photoactivation. *Journal of Medicinal Chemistry* **61(14)**:6211–6235 DOI [10.1021/acs.jmedchem.8b00629](https://doi.org/10.1021/acs.jmedchem.8b00629).
- Lutz T, Wein T, Höfner G, Wanner KT. 2017.** Development of highly potent GAT1 inhibitors: synthesis of nipecotic acid derivatives with N-arylalkynyl substituents. *ChemMedChem* **12(5)**:362–371 DOI [10.1002/cmdc.201600599](https://doi.org/10.1002/cmdc.201600599).

- Madsen KK, Ebert B, Clausen RP, Krogsgaard-Larsen P, Schousboe A, White HS. 2011.** Selective GABA transporter inhibitors tiagabine and EF1502 exhibit mechanistic differences in their ability to modulate the ataxia and anticonvulsant action of the extrasynaptic GABA<sub>A</sub> receptor agonist gaboxadol. *Journal of Pharmacology and Experimental Therapeutics* **338**(1):214–219 DOI [10.1124/jpet.111.179671](https://doi.org/10.1124/jpet.111.179671).
- Magrane M. 2011.** UniProt Knowledgebase: a hub of integrated protein data. *Database* **2011**:bar009 DOI [10.1093/database/bar009](https://doi.org/10.1093/database/bar009).
- Martin YC, Bures MG, Danaher EA, Delazzer J, Lico I, Pavlik PA. 1993.** A fast new approach to pharmacophore mapping and its application to dopaminergic and benzodiazepine agonists. *Journal of Computer-Aided Molecular Design* **7**(1):83–102 DOI [10.1007/BF00141577](https://doi.org/10.1007/BF00141577).
- Melone M, Ciappelloni S, Conti F. 2015.** A quantitative analysis of cellular and synaptic localization of GAT-1 and GAT-3 in rat neocortex. *Brain Structure and Function* **220**(2):885–897 DOI [10.1007/s00429-013-0690-8](https://doi.org/10.1007/s00429-013-0690-8).
- Minelli A, Brecha NC, Karschin C, DeBiasi S, Conti F. 1995.** GAT-1, a high-affinity GABA plasma membrane transporter, is localized to neurons and astroglia in the cerebral cortex. *Journal of Neuroscience* **15**(11):7734–7746 DOI [10.1523/JNEUROSCI.15-11-07734.1995](https://doi.org/10.1523/JNEUROSCI.15-11-07734.1995).
- Minelli A, DeBiasi S, Brecha NC, Zuccarello LV, Conti F. 1996.** GAT-3, a high-affinity GABA plasma membrane transporter, is localized to astrocytic processes, and it is not confined to the vicinity of GABAergic synapses in the cerebral cortex. *Journal of Neuroscience* **16**(19):6255–6264 DOI [10.1523/JNEUROSCI.16-19-06255.1996](https://doi.org/10.1523/JNEUROSCI.16-19-06255.1996).
- Minh BQ, Klaere S, von Haeseler A. 2009.** Taxon selection under split diversity. *Systematic Biology* **58**(6):586–594 DOI [10.1093/sysbio/syp058](https://doi.org/10.1093/sysbio/syp058).
- Nakada K, Yoshikawa M, Ide S, Suemasa A, Kawamura S, Kobayashi T, Masuda E, Ito Y, Hayakawa W, Katayama T, Yamada S, Arisawa M, Minami M, Shuto S. 2013.** Cyclopropane-based conformational restriction of GABA by a stereochemical diversity-oriented strategy: identification of an efficient lead for potent inhibitors of GABA transports. *Bioorganic & Medicinal Chemistry* **21**(17):4938–4950 DOI [10.1016/j.bmc.2013.06.063](https://doi.org/10.1016/j.bmc.2013.06.063).
- Nowaczyk A, Fijałkowski Ł., Kowalska M, Podkowa A, Sałat K. 2018.** Studies on the activity of selected highly lipophilic compounds toward hGAT1 inhibition. Part II. Epub ahead of print 28 September 2018. *ACS Chemical Neuroscience* DOI [10.1021/acschemneuro.8b00282](https://doi.org/10.1021/acschemneuro.8b00282).
- Parpura V, Haydon PG. 2008.** *Astrocytes in (patho) physiology of the nervous system*. New York: Springer.
- Petrera M, Wein T, Allmendinger L, Sindelar M, Pabel J, Höfner G, Wanner KT. 2015.** Development of highly potent GAT1 inhibitors: synthesis of nipecotic acid derivatives by Suzuki-Miyaura cross-coupling reactions. *ChemMedChem* **11**(5):519–538 DOI [10.1002/cmdc.201500490](https://doi.org/10.1002/cmdc.201500490).
- Pirttimäki T, Parri HR, Crunelli V. 2013.** Astrocytic GABA transporter GAT-1 dysfunction in experimental absence seizures. *Journal of physiology* **591**(4):823–833 DOI [10.1113/jphysiol.2012.242016](https://doi.org/10.1113/jphysiol.2012.242016).
- Pizzi DA, Leslie CP, Fabio RD, Seri C, Bernasconi G, Squaglia M, Carnevale G, Falchi A, Greco E, Mangiarini L, Negri M. 2011.** Stereospecific synthesis and structure–activity relationships of unsymmetrical 4,4-diphenylbut-3-enyl derivatives of nipecotic acid as GAT-1 inhibitors. *Bioorganic & Medicinal Chemistry Letters* **21**(1):602–605 DOI [10.1016/j.bmcl.2010.09.025](https://doi.org/10.1016/j.bmcl.2010.09.025).
- Quandt G, Höfner G, Wanner KT. 2013.** Synthesis and evaluation of N-substituted nipecotic acid derivatives with an unsymmetrical bis-aromatic residue attached to a vinyl ether spacer as

- potential GABA uptake inhibitors. *Bioorganic & Medicinal Chemistry* **21(11)**:3363–3378 DOI [10.1016/j.bmc.2013.02.056](https://doi.org/10.1016/j.bmc.2013.02.056).
- Reith ME. 2007. *Handbook of neurochemistry and molecular neurobiology: neural membranes and transport*. New York: Springer Science and Business Media.
- Rud E, Gederaas O, Høgset A, Berg K. 2000. 5-aminolevulinic acid, but not 5-aminolevulinic acid esters, is transported into adenocarcinoma cells by system BETA transporters. *Photochemistry and Photobiology* **71**:640–647 DOI [10.1562/0031-8655\(2000\)071<0640:AABNAA>2.0.CO;2](https://doi.org/10.1562/0031-8655(2000)071<0640:AABNAA>2.0.CO;2).
- Sadowski J. 2003. 3D structure generation. *Handbook of Chemoinformatics: from Data to Knowledge in 4 volumes*. Weinheim: Wiley-VCH, 231–261.
- Sadowski J, Schwab CH, Gasteiger J. 2004. *3D structure generation and conformational searching*. New York: Dekker Inc.
- Śałat K, Podkowa A, Malikowska N, Kern F, Pabel J, Wojcieszak E, Kulig K, Wanner KT, Strach B, Wyska E. 2017. Novel, highly potent and *in vivo* active inhibitor of GABA transporter subtype 1 with anticonvulsant, anxiolytic, antidepressant and antinociceptive properties. *Neuropharmacology* **113**:331–342 DOI [10.1016/j.neuropharm.2016.10.019](https://doi.org/10.1016/j.neuropharm.2016.10.019).
- Šali A, Potterton L, Yuan F, van Vlijmen H, Karplus M. 1995. Evaluation of comparative protein modeling by MODELLER. *Proteins: Structure, Function, and Bioinformatics* **23(3)**:318–326 DOI [10.1002/prot.340230306](https://doi.org/10.1002/prot.340230306).
- Schmidt SK, Höfner G, Wanner KT. 2017. Determination of enantiomeric excess of nipecotic acid as 1-(7-nitrobenzo [c][1, 2, 5] oxadiazol-4-yl) derivatives. *Chirality* **29(1)**:48–56 DOI [10.1002/chir.22670](https://doi.org/10.1002/chir.22670).
- Schmuker M, Givhchi A, Schneider G. 2004. Impact of different software implementations on the performance of the Maxmin method for diverse subset selection. *Molecular Diversity* **8(4)**:421–425 DOI [10.1023/B:MODI.0000047503.82461.e8](https://doi.org/10.1023/B:MODI.0000047503.82461.e8).
- Schousboe A. 2000. Pharmacological and functional characterization of astrocytic GABA transport: a short review. *Neurochemical Research* **25(9/10)**:1241–1244 DOI [10.1023/A:1007692012048](https://doi.org/10.1023/A:1007692012048).
- Schrödinger. 2017. Schrödinger software release 2017-1. Available at <https://www.schrodinger.com/news/announcing-schr%C3%B6dinger-software-release-2017-1>.
- Sherin JE, Nemeroff CB. 2011. Post-traumatic stress disorder: the neurobiological impact of psychological trauma. *Dialogues in Clinical Neuroscience* **13**:263.
- Sherman W, Day T, Jacobson MP, Friesner RA, Farid R. 2006. Novel procedure for modeling ligand/receptor induced fit effects. *Journal of Medicinal Chemistry* **49(2)**:534–553 DOI [10.1021/jm050540c](https://doi.org/10.1021/jm050540c).
- Shetty AK, Bates A. 2015. Potential of GABA-ergic cell therapy for schizophrenia, neuropathic pain, and Alzheimer's and Parkinson's diseases. *Brain Research* **1638**:74–87 DOI [10.1016/j.brainres.2015.09.019](https://doi.org/10.1016/j.brainres.2015.09.019).
- Sitka I, Allmendinger L, Fülep G, Höfner G, Wanner KT. 2013. Synthesis of N-substituted acyclic  $\beta$ -amino acids and their investigation as GABA uptake inhibitors. *European Journal of Medicinal Chemistry* **65**:487–499 DOI [10.1016/j.ejmech.2013.04.063](https://doi.org/10.1016/j.ejmech.2013.04.063).
- Skovstrup S, Taboureau O, Bräuner-Osborne H, Jørgensen FS. 2010. Homology modelling of the GABA transporter and analysis of tiagabine binding. *ChemMedChem* **5(7)**:986–1000 DOI [10.1002/cmdc.201000100](https://doi.org/10.1002/cmdc.201000100).
- Stanton DT, Morris TW, Roychoudhury S, Parker CN. 1999. Application of nearest-neighbor and cluster analyses in pharmaceutical lead discovery. *Journal of Chemical Information and Computer Sciences* **39(1)**:21–27 DOI [10.1021/ci9801015](https://doi.org/10.1021/ci9801015).

- Tóth K, Höfner G, Wanner KT. 2018.** Synthesis and biological evaluation of novel N-substituted nipecotinic acid derivatives with a trans-alkene spacer as potent GABA uptake inhibitors. *Bioorganic & Medicinal Chemistry* **26(22)**:5944–5961 DOI [10.1016/j.bmc.2018.11.002](https://doi.org/10.1016/j.bmc.2018.11.002).
- Wang KH, Penmatsa A, Gouaux E. 2015a.** Neurotransmitter and psychostimulant recognition by the dopamine transporter. *Nature* **521(7552)**:322–327 DOI [10.1038/nature14431](https://doi.org/10.1038/nature14431).
- Wang KH, Penmatsa A, Gouaux E. 2015b.** Neurotransmitter and psychostimulant recognition by the dopamine transporter. *Nature* **521(7552)**:322–327 DOI [10.1038/nature14431](https://doi.org/10.1038/nature14431).
- Wermuth PBCG. 2008.** *The Practice of Medicinal Chemistry*. Amsterdam: Elsevier BV, 319–357.
- Yamashita A, Singh S, Kawate T, Jin Y, Gouaux E. 2005.** Crystal structure of a bacterial homologue of Na<sup>+</sup>/Cl<sup>-</sup> (-dependent neurotransmitter transporters. *Nature* **437(7056)**:215–223 DOI [10.1038/nature03978](https://doi.org/10.1038/nature03978).
- Yu N, Cao Y, Mager S, Lester HA. 1998.** Topological localization of cysteine 74 in the GABA transporter, GAT1, and its importance in ion binding and permeation. *FEBS Letters* **426(2)**:174–178 DOI [10.1016/S0014-5793\(98\)00333-0](https://doi.org/10.1016/S0014-5793(98)00333-0).
- Zafar S, Jabeen I. 2018.** Structure, function, and modulation of  $\gamma$ -aminobutyric acid transporter 1 (GAT1) in neurological disorders: a pharmacoinformatic prospective. *Frontiers in Chemistry* **6**:397 DOI [10.3389/fchem.2018.00397](https://doi.org/10.3389/fchem.2018.00397).
- Zhao X, Hoegl CE, Hoefner GC, Wanner KT. 2005.** Synthesis and biological evaluation of new GABA-uptake inhibitors derived from proline and from pyrrolidine-2-acetic acid. *European Journal of Medicinal Chemistry* **40(3)**:231–247 DOI [10.1016/j.ejmech.2004.11.004](https://doi.org/10.1016/j.ejmech.2004.11.004).
- Zheng J, Wen R, Luo X, Lin G, Zhang J, Xu L, Guo L, Jiang H. 2006.** Design, synthesis, and biological evaluation of the N-diarylalkenyl-piperidinecarboxylic acid derivatives as GABA uptake inhibitors (I). *Bioorganic & Medicinal Chemistry Letters* **16(1)**:225–227 DOI [10.1016/j.bmcl.2005.09.004](https://doi.org/10.1016/j.bmcl.2005.09.004).
- Zhou Y, Zomot E, Kanner BI. 2006.** Identification of a lithium interaction site in the  $\gamma$ -aminobutyric acid (GABA) transporter GAT-1. *Journal of Biological Chemistry* **281(31)**:22092–22099 DOI [10.1074/jbc.M602319200](https://doi.org/10.1074/jbc.M602319200).